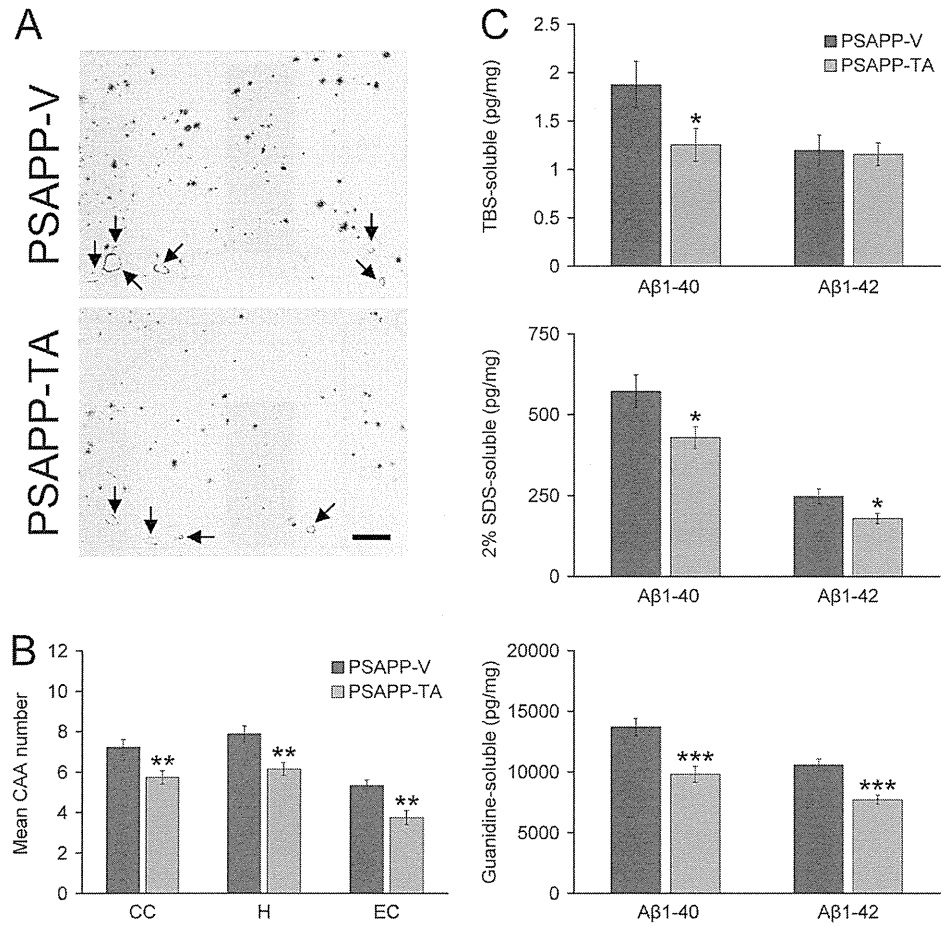

FIGURE 4. **Cerebral vascular β-amyloid deposits and brain Aβ levels are reduced in PSAPP mice given oral tannic acid treatment.** *A,* representative photomicrographs of 4G8 immunohistochemistry were taken from PSAPP-V and PSAPP-TA mouse hippocampi at 12 months of age, and cerebral vascular β-amyloid deposits are indicated (*arrows*). *Scale bar* denotes 200 μm. *B,* severity of cerebral amyloid angiopathy (mean CAA deposit number per mouse) is shown on the *y* axis with the brain region indicated on the *x* axis (*CC, H,* and *EC*). *C,* TBS-soluble, 2% SDS-soluble, and TBS-insoluble (but 5 M guanidine HCl-extractable) fractions from three-step extracted brain homogenates were examined by sandwich ELISA for human $A\beta_{1-40}$ and $A\beta_{1-42}$ levels. Data were obtained from PSAPP mice treated with vehicle (*PSAPP-V, n* = 16) or with TA (*PSAPP-TA, n* = 16) for 6 months commencing at 6 months of age. All statistical comparisons are within the brain region and/or between PSAPP-V and PSAPP-TA mice.

By contrast, $A\beta_{1-42}$ levels in the TBS-soluble fraction were similar between PSAPP-TA and PSAPP-V mice. We also analyzed PSAPP-6M mice by Aβ biochemistry, but found low abundance of Aβ species that was below the threshold of ELISA detection in certain fractions (data not shown). Collectively, these data show that cerebral amyloidosis, including brain parenchymal and cerebral vascular β-amyloid deposits and Aβ peptide abundance, is delayed but not completely prevented by oral treatment with TA in PSAPP mice.

Inhibition of Cerebral Amyloidogenic APP Metabolism in Tannic Acid-treated PSAPP Mice—Mitigated cerebral amyloidosis in PSAPP-TA mice could be due to 1) increased brain-to-blood Aβ efflux (10), 2) reduced expression of APP or PS1 transgenes, or 3) attenuated amyloidogenic APP metabolism. We obtained peripheral blood samples from PSAPP-V and PSAPP-TA mice at the time of sacrifice and assayed plasma $A\beta_{1-40}$ and $A\beta_{1-42}$ species, but did not detect differences between groups (data not shown). To examine if TA-attenuated cerebral amyloidosis could be due to decreased expression of transgene-derived APP or PS1, we probed brain homogenates from PSAPP-V and PSAPP-TA mice using amino-terminal APP polyclonal or carboxyl-terminal PS1 monoclonal antibodies and found no change in APP or PS1 holoprotein levels (Fig. 5*A* and data not shown).

To determine whether APP metabolites including sAPP-α and sAPP-β were affected by TA treatment, brain homogenates were probed with monoclonal antibody 2B3 that detects the carboxyl terminus of human sAPP-α and with monoclonal antibody 6A1 that recognizes the carboxyl terminus of human Swedish mutant sAPP-β. Western blot and densitometry data showed significantly reduced expression of sAPP-β in PSAPP-TA mouse brains, whereas sAPP-α abundance did not differ between groups (Fig. 5, *A–C*, ***, $p < 0.001$). To further determine whether amyloidogenic APP processing was inhibited by TA treatment, we probed brain homogenates with a carboxyl-terminal BACE1 polyclonal antibody. Densitometry showed that BACE1 protein abundance was significantly decreased in PSAPP-TA mice (Fig. 5, *A* and *D*, *, $p < 0.05$). To assess whether this effect was due to TA attenuation of BACE1 transcription, relative expression levels of BACE1 mRNA were assayed in each mouse group by QPCR. However, there were no detectable differences between groups (Fig. 5*E*), suggesting a post-transcriptional mode of TA action on BACE1.

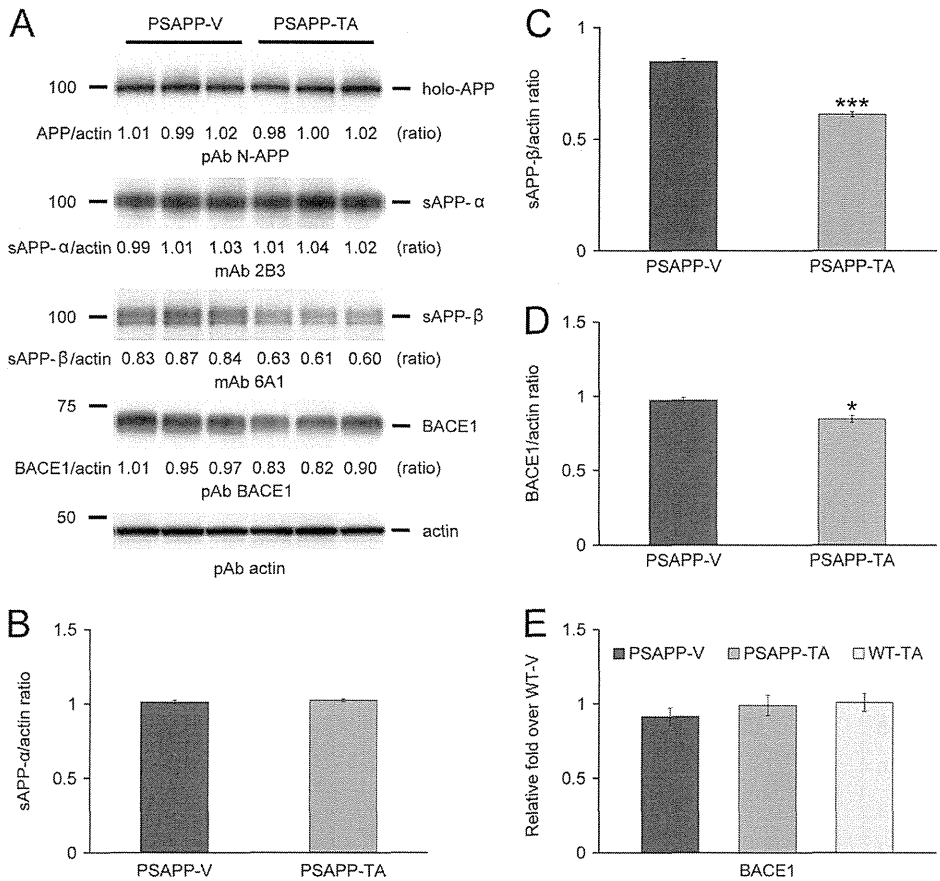

FIGURE 5. **Tannic acid inhibits BACE1 protein at the post-transcriptional level in PSAPP mice.** *A*, Western blots are shown using an amino (N)-terminal APP polyclonal antibody (*pAb N-APP*; holo-APP is shown), a carboxyl-terminal human sAPP-α monoclonal antibody (*mAb 2B3*; sAPP-α is shown), a carboxyl-terminal human sAPP-β monoclonal antibody (*mAb 6A1*; sAPP-β is shown), and a carboxyl-terminal β-site APP cleaving enzyme 1 polyclonal antibody (*pAb BACE1*). Actin is shown as a loading control for each blot. Densitometry analyses are shown for the ratio of: *B*, sAPP-α to actin; *C*, sAPP-β to actin; and *D*, BACE1 to actin. *E*, QPCR data reveal no differences between groups on BACE1 expression. Data are expressed as relative fold over WT-V mice. Data for *A–D* were obtained from PSAPP mice treated with vehicle (*PSAPP-V*, $n = 16$) or with TA (*PSAPP-TA*, $n = 16$) for 6 months beginning at 6 months of age. Wild-type mice treated with vehicle (*WT-V*, $n = 16$) or with TA (*WT-TA*, $n = 16$) were also included for *E*. The statistical comparisons for *C* and *D* are between PSAPP-V and PSAPP-TA mice.

To further address steady-state APP metabolism, we probed brain homogenates with monoclonal antibody 82E1 that recognizes amino acids 1–16 of human Aβ, and detects the amyloidogenic β-CTF (C-99) and phospho-β-CTF (P-C99) and monomeric plus oligomeric Aβ species. Densitometry confirmed that APP metabolism to phospho-C99 and C99 was significantly deceased in PSAPP-TA mice (Fig. 6, *A* and *B*, **, $p < 0.01$). These effects were accompanied by reduced abundance of the Aβ species between 25 and 75 kDa (presumed Aβ oligomers) and monomeric Aβ in PSAPP-TA mice (Fig. 6*A*). To confirm that Aβ oligomers were attenuated by TA treatment, we quantified them in the detergent-soluble fraction by sandwich ELISA and found significant reduction in PSAPP-TA *versus* PSAPP-V mice (Fig. 6*C*, *, $p < 0.05$). Collectively, these data indicate that TA works at the protein level to inhibit BACE1 expression. Consistently, β-secretase activity was significantly decreased, whereas α-secretase activity was unaltered in brain homogenates from PSAPP-TA *versus* PSAPP-V mice (Fig. 6*D*, ***, $p < 0.001$ at each time point). These data support the notion that TA affords prophylaxis against cerebral amyloidosis by inhibiting amyloidogenic APP metabolism as a consequence of decreasing BACE1 expression at the protein (but not mRNA) level and reducing β-secretase activity.

Tannic Acid Reduces Aβ Production and Inhibits Amyloidogenic APP Metabolism in Neuron-like Cells—Mitigated cerebral amyloidosis and reduced amyloidogenic APP metabolism in PSAPP-TA mice could be due to a direct, neuron cell autonomous affect or to an indirect mode of TA action. To determine whether TA could directly modulate APP metabolism in neuron-like cells, we cultured SweAPP N2a cells, which stably express human APP bearing the Swedish mutation, and treated them with a dose-range of TA. As shown in Fig. 7*A*, TA dose dependently inhibited both $A\beta_{1-40}$ and $A\beta_{1-42}$ release into the media by separate sandwich ELISAs. Although the optimal effect occurred at 12.5 μM, significant reduction for both Aβ peptides was evident even at the lowest dose (3.125 μM) of TA used (*, $p < 0.05$; **, $p < 0.01$ for each dose *versus* PBS control).

We moved on to investigate whether these effects were because of reduced amyloidogenic APP metabolism, and performed Western blots with a carboxyl-terminal APP polyclonal antibody that simultaneously detects both amyloidogenic C99 and nonamyloidogenic C83 (α-carboxyl-terminal fragment, α-CTF) (Fig. 7*B*). Results qualitatively showed less abundance of C99 with increasing doses of TA. Quantitative densitometry followed by one-way ANOVA revealed a significant main effect of dose ($p < 0.01$), and post hoc testing revealed significant

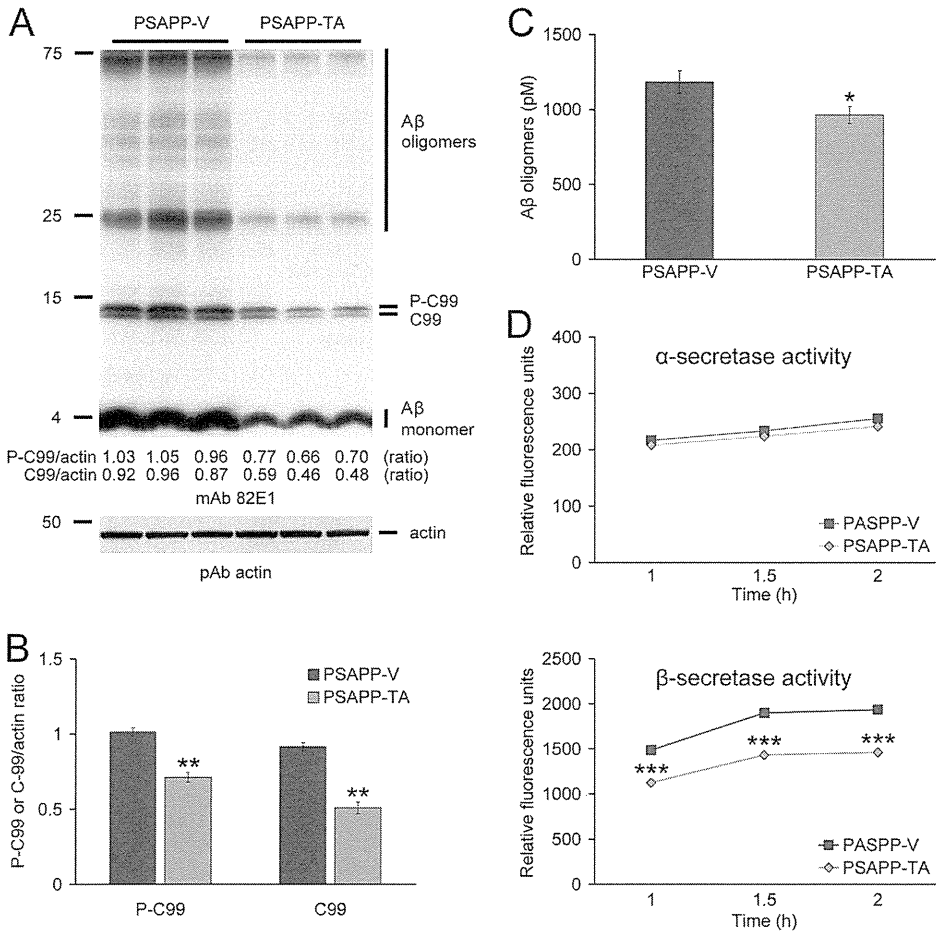

FIGURE 6. **Anti-amyloidogenic APP processing in PSAPP mice treated with tannic acid.** *A*, Western blots using an amino-terminal Aβ monoclonal antibody (*mAb 82E1*) are shown. This antibody detects various fragments generated by amyloidogenic APP cleavage, including: Aβ oligomers and monomer as well as phospho-C99 (*P-C99*) and non-phospho-C99 (*C99*). Actin is shown as a loading control. *B*, densitometry analysis is shown for ratios of C-99 or P-C99 to actin. *C*, the levels of Aβ oligomers in the 2% SDS-soluble brain homogenate fraction were measured by sandwich ELISA. *D*, α-secretase and β-secretase activity assays are shown. Relative fluorescence units are shown on the *y* axis, and reaction time is represented on the *x* axis. Data for *A–D* were obtained from PSAPP mice treated with vehicle (*PSAPP-V*, $n = 16$) or with TA (*PSAPP-TA*, $n = 16$) for 6 months beginning at 6 months of age. The statistical comparisons for *B–D* are between PSAPP-V and PSAPP-TA mice.

differences when comparing control (PBS-treated) SweAPP N2a cells to cells that were treated with 12.5 to 25 μM TA (Fig. 7*C*, *, $p < 0.05$). To determine whether BACE1 protein levels were reduced by TA treatment, we probed brain homogenates with a carboxyl-terminal BACE1 polyclonal antibody. Results showed TA dose-dependent inhibition of BACE1 protein (Fig. 7*D*).

To determine whether TA directly or indirectly inhibited BACE1 activity, we developed a BACE1 activity assay consisting of combining a dose range of TA in a cell-free system with BACE1 enzyme and fluorogenic reporters. The result was positive, as one-way ANOVA revealed a significant main effect of TA dose ($p < 0.001$) and post hoc testing revealed significant differences when comparing BACE1 enzyme alone (positive control) to samples that contained from 1.563 to 25 μM TA. Of note, significant reduction for BACE1 activity was evident even at the lowest dose (1.563 μm) of TA used (Fig. 7*E*, **, $p < 0.01$). BACE1 inhibitor II treatment (used as a BACE1 inhibitor control; $IC_{50} = 0.97$ μM) at 1.25 μM revealed an inhibitory effect for BACE1 (497.3 ± 8.8 relative fluorescence units) as compared with 100% BACE1 enzyme activity (646.3 ± 25.4 relative fluorescence units). Interestingly, this effect was quantitatively more minor than even the lowest dose of TA used in this system.

Finally, to determine whether escalating doses of TA were toxic to SweAPP N2a cells, we performed a lactate dehydrogenase release assay, but did not observe evidence of TA toxicity (Fig. 7*F*). When taken together, these data show that TA is capable of exerting a direct effect on reducing Aβ secretion and amyloidogenic APP metabolism in neuron-like cells.

Tannic Acid Attenuates Neuroinflammation in PSAPP Mice—Chronic activation of glial cells in and around β-amyloid plaques may be pathoetiologic in AD via production of numerous neurotoxic acute-phase reactants, proinflammatory cytokines, and immunostimulatory molecules (53, 54). Furthermore, neuroinflammation, as earmarked by β-amyloid plaque-associated reactive gliosis and increased expression of proinflammatory cytokines, has been demonstrated in aged transgenic mouse models of cerebral amyloid deposition (18, 42, 43, 55–57). To test whether TA impacted neuroinflammatory processes in PSAPP mice, we examined β-amyloid plaque-associated microgliosis (by Iba1 antibody) and astrocytosis (using GFAP antibody) immunoreactivity

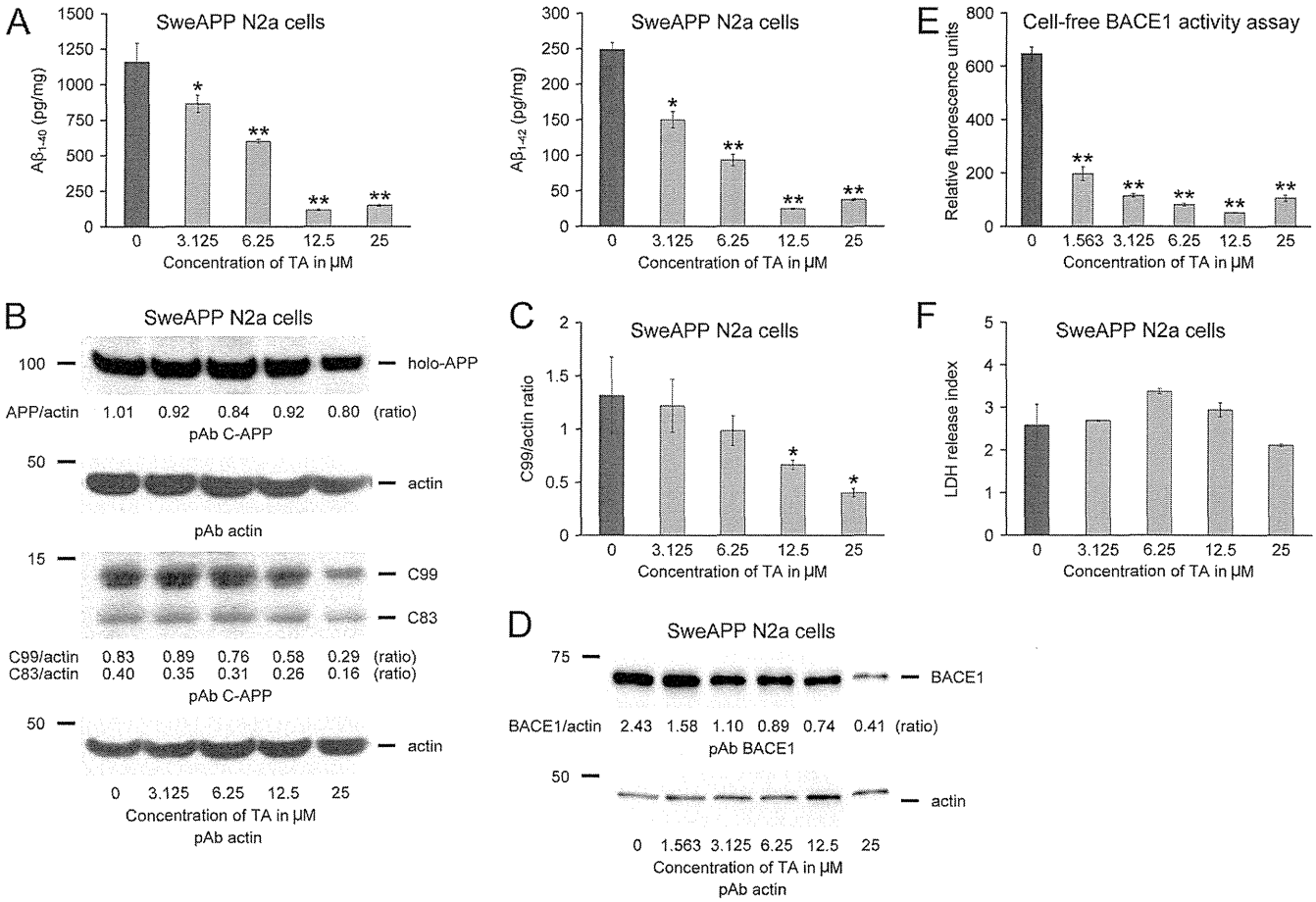

FIGURE 7. **Tannic acid reduces Aβ production and inhibits amyloidogenic APP metabolism in SweAPP N2a cells, and directly inhibits BACE1 in a cell-free system.** *A*, $A\beta_{1-40}$ and $A\beta_{1-42}$ species in cell supernatants from SweAPP N2a cells were separately measured by sandwich ELISA. *B*, promotion of anti-amyloidogenic APP processing in SweAPP N2a cells treated with TA. Western blots using a carboxyl-terminal APP polyclonal antibody (*pAb C-APP*) show holo-APP and carboxyl-terminal fragments generated by amyloidogenic APP cleavage (*C99*, β-CTF and *C83*, α-CTF). Actin is included as an internal reference control. *C*, densitometry analyses for the ratio of C99 to actin at various TA treatment doses are shown. *D*, BACE1 expression is inhibited in SweAPP N2a cells treated with TA. A representative pAb BACE1 Western blot is shown. Actin is included as an internal reference control, and ratiometric densitometry data are shown *below* each lane. *E*, cell-free BACE1 activity assay results are shown. Relative fluorescence units are shown on the *y* axis. *F*, lactate dehydrogenase (*LDH*) release assay for SweAPP N2a cells treated from 0 to 25 μM of TA. All statistical comparisons are *versus* 0 μM of TA, and similar results were observed in 2–3 independent experiments.

(conventional microgliosis and astrocytosis burden analyses) and quantified brain expression of the proinflammatory cytokines TNF-α and IL-1β. PSAPP-V mice demonstrated elevated β-amyloid plaque-associated reactive gliosis (microgliosis and astrocytosis), as evidenced by increased expression of Iba1 and GFAP in glial somata and processes. Yet, microgliosis and astrocytosis were significantly reduced in PSAPP-TA mice compared with PSAPP-V animals (Figs. 8, *A* and *B*, and 9, *A* and *B*, ***, $p < 0.001$). These effects were gender-independent, as a similar pattern of statistically significant results was observed in both male and female PSAPP-TA mice (data not shown). When considering brain mRNA abundance of TNF-α and IL-1β, a similar pattern of statistically significant results was found (Fig. 9*C*, **, $p < 0.01$). Neuroinflammation in PSAPP-TA mice was not reduced to levels of untreated PSAPP-6M mice, indicating mitigation but not complete prevention of this pathology (Figs. 8, *A* and *B*, and 9, *A–C*).

Phagocytic microglia have been detected in the aged APP23 cerebral amyloidosis mouse model in small numbers (58) and in increased abundance in aged Tg2576 mice bearing a CD11c promoter-driven dominant-negative transforming growth factor-β receptor type II transgene (18) as well as in the ischemic core after cerebral ischemia in the rat brain (59). However, reactive microglia in both groups of mice reported here had ramified thin and long cell processes and did not appear to be phagocytic based on morphological criteria (amoeboid structure, puffy cytoplasm, few or no processes resembling brain-infiltrating macrophages) (60).

DISCUSSION

Nutraceuticals are naturally occurring compounds that, because of their existence throughout evolution, tend to have fewer side effects than designer pharmaceuticals. The purpose of the present study was to evaluate the effects of TA, a plant-derived flavonoid nutraceutical, on behavioral impairment, AD-like pathology, and APP metabolism *in vivo* and *in vitro*. Collectively, our results demonstrate that oral TA prevents behavioral impairment, mitigates cerebral amyloidosis, and promotes nonamyloidogenic APP processing by inhibiting BACE1 expression and β-secretase activity without altering BACE1 mRNA abundance in an accelerated mouse model of

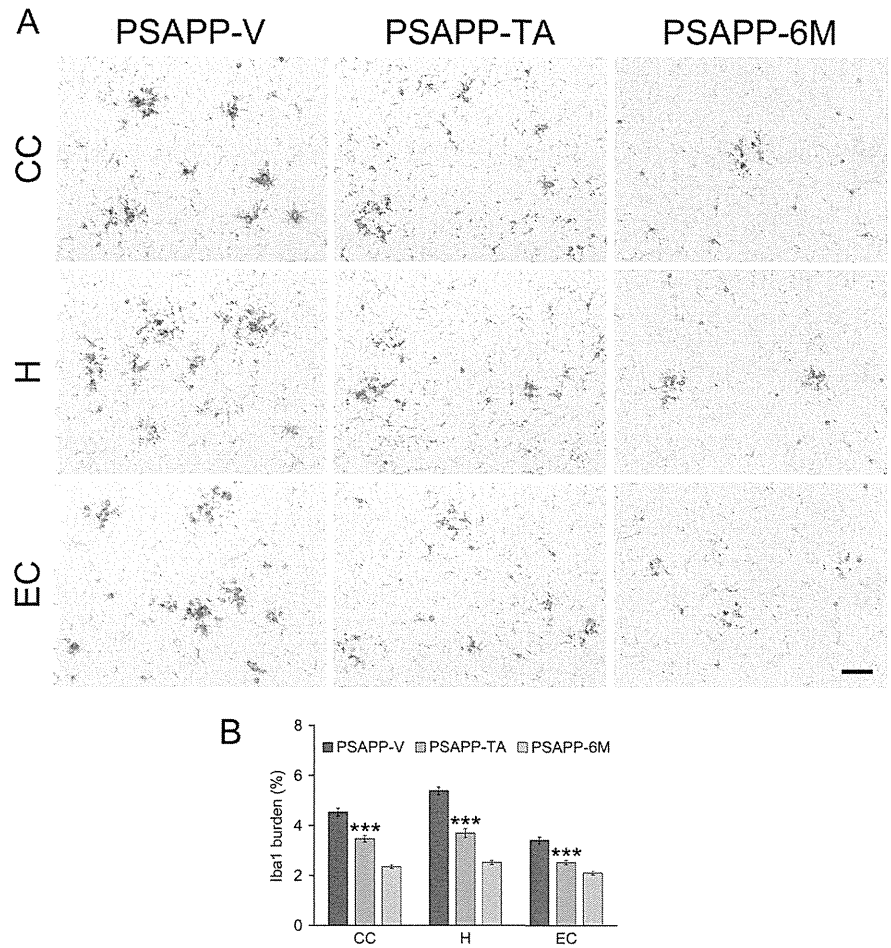

FIGURE 8. **Attenuated reactive microgliosis in PSAPP mice treated with tannic acid.** Data were obtained from PSAPP mice treated with vehicle (*PSAPP-V*, $n = 16$) or with TA (*PSAPP-TA*, $n = 16$) for 6 months commencing at 6 months of age. In addition, untreated PSAPP mice at 6 months of age (*PSAPP-6M*, $n = 12$) were included in the analysis. *A*, representative photomicrographs of Iba1 immunohistochemistry for β-amyloid plaque-associated microgliosis are shown in PSAPP-V and PSAPP-TA mice at 12 months of age as well as in PSAPP-6M mice. Brain regions shown include *CC* (*top*), *H* (*middle*), and *EC* (*bottom*). *Scale bar* denotes 50 μm. *B*, quantitative image analysis for Iba1 burden is shown for each brain region indicated on the *x* axis. All statistical comparisons are *versus* PSAPP-TA mice.

cerebral amyloid deposition. In addition, TA dose-dependently inhibited $A\beta_{1-40}$ and $A\beta_{1-42}$ production and β-CTF cleavage in human SweAPP-expressing neuron-like cells *in vitro*. Finally, TA attenuated neuroinflammation in PSAPP mice, including β-amyloid plaque-associated gliosis and expression of the pro-inflammatory cytokines TNF-α and IL-1β.

TA is a member of the tannin category of plant-derived polyphenols, and is found in numerous herbaceous and woody plants. Tannins are chemically divided into four groups based on the structure of the monomer: hydrolysable tannins, condensed tannins (proanthocyanidins), phlorotannins, and complex tannins. Among these, hydrolyzable tannins (including TA) are derivatives of gallic acid (3,4,5-trihydroxyl benzoic acid), characterized by a variable number of gallate moieties esterified to a core phenol (29). Similar to other polyphenols, tannins have antioxidant/free radical scavenging, antiviral/bacterial, anticarcinogenic, antimutagenic, and anti-inflammatory properties (29, 61–63). Given these pleiotropic biological activities, TA has yielded promising clinical results against cancer (61), myocardial infarction (64), and renal failure (65).

In this study, we orally administered TA to mice at 30 mg/kg/day via gavage, as this treatment strategy more precisely delivers the targeted amount of agent compared with *ad libitum* access in drinking water or chow. TA is well tolerated in rodents, with a lethal dose resulting in 50% mortality as high as 2,260 mg/kg in the rat (66), and the dose that we administered to mice is orders of magnitude lower. Similarly, the human tolerable daily intake of TA is 13.6 g/60 kg (67). Unwanted side effects are always a concern in the clinic, and it is important to note that we did not observe evidence for adverse events associated with TA treatment in mice, including abnormal behavior, altered body weight or food intake, or mortality. Likewise, we did not detect pathological features in major organs such as the brain, lung, heart, liver, digestive tract, and kidney upon postmortem examination of TA-treated PSAPP or WT mice. These findings reinforce the notion that the dose of TA used in our study is safe; of course, our results are limited to mice. Because BACE1 likely has important physiologic functions, and TA may have long-term toxic effects due to inhibition of BACE1, possible side effects of TA would need to be properly investigated in humans.

It is important to consider how TA exerts its biological effects. The compound is a high molecular weight molecule that does not easily penetrate the cell or freely cross the blood-

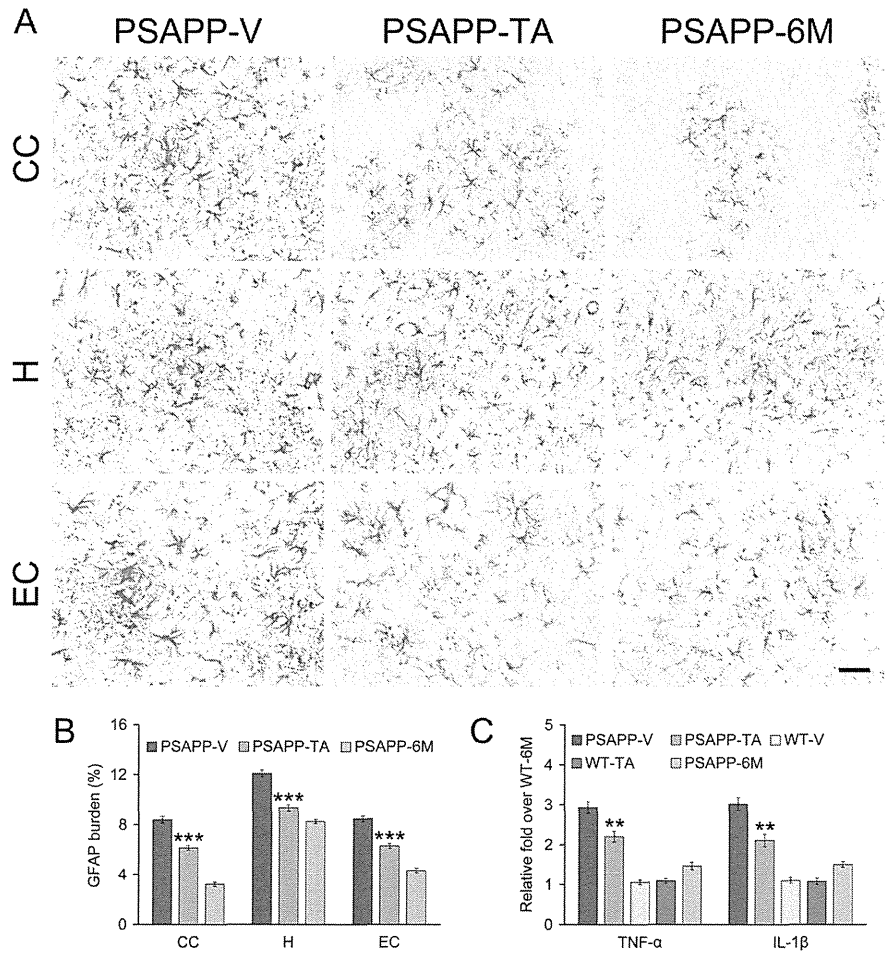

FIGURE 9. **Tannic acid-treated PSAPP mice have reduced astrocytosis.** Data for *A* and *B* were obtained from PSAPP mice treated with vehicle (*PSAPP-V*, $n = 16$) or with TA (*PSAPP-TA*, $n = 16$) for 6 months beginning at 6 months of age. In addition, 6-month-old untreated PSAPP mice (*PSAPP-6M*, $n = 12$) and wild-type (*WT-6M*, $n = 12$) mice were included for *C*. *A*, representative photomicrographs of GFAP immunohistochemistry, taken from each brain region indicated on the *left* (*CC*, *top*; *H*, *middle*; *EC*, *bottom*), for β-amyloid plaque-associated astrocytosis are shown for PSAPP-V and PSAPP-TA mice at 12 months of age and for untreated PSAPP-6M mice. *Scale bar* denotes 50 μm. *B*, quantitative image analysis for GFAP burden is shown for each brain region indicated on the *x* axis. *C*, expression of brain proinflammatory TNF-α and IL-1β cytokine mRNAs is attenuated by TA treatment in PSAPP mice. Data are expressed as relative fold over WT-6M mice, and all statistical comparisons are *versus* PSAPP-TA mice.

brain barrier. Nonetheless, TA is metabolized into much lower molecular weight, absorbable tannins that are biologically active in various organs including the brain (68). For example, hydrolysable tannins are degraded to gallic acid, pyrogallol, phloroglucinol, and finally to acetate and butyrate via sequential enzymatic action (29). In particular, oral administration of gallic acid led to intestinal absorption over a period of ~60 min in rodents (69), which equated to 76 min in humans (70). Flavonoids including gallate have also been shown to cross into the brain in rodents (68, 71, 72). Thus, the gallate moiety is a likely candidate for mediating the bioactivity of TA in our system; yet, future study is warranted to characterize which chemical structure in TA plays a pivotal role on mitigating Aβ pathology.

Our *in vivo* and *in vitro* results show that TA shifts APP metabolism toward the nonamyloidogenic pathway. Specifically, TA lowered BACE1 expression (without any change in BACE1 mRNA expression) and β-secretase activity (but had no effect on α-secretase activity), leading to reduced abundance of the amyloidogenic C99 and phospho-C99 APP CTFs, attenuated sAPP-β abundance, and lower levels of Aβ peptides. Interestingly, TA exerts its effects on BACE1 both at the post-translational level and also by directly attenuating enzymatic activity, as demonstrated in a cell-free BACE1 activity assay. Although Aβ is generally regarded as the pathogenic species in both mouse models of cerebral amyloidosis and in human AD, it remains possible that TA reduction of any combination of amyloidogenic APP metabolites may be responsible for bringing about reduced behavioral impairment in PSAPP mice.

It is generally recognized that APP is a limiting reagent in the cell, and it has been postulated that α- and β-secretases compete for APP proteolysis (73). Reduced β-secretase activity could therefore be responsible for mitigated cerebral Aβ pathology in TA-treated PSAPP mice and attenuated Aβ secretion by SweAPP N2a cells. In this regard, we previously demonstrated that another polyphenol, EGCG (a bioactive flavonoid ingredient in green tea), was also able to promote nonamyloidogenic APP metabolism in the Tg2576 cerebral amyloidosis mouse model and in SweAPP N2a cells (23). Interestingly, the mechanism for the beneficial effects of EGCG on nonamyloidogenic APP processing relied on promoting activity

of the candidate α-secretase, a disintegrin and metalloprotease 10 (23, 24). Given their complementary modes of action then, a combined TA/EGCG approach may make sense, at least in principle, as an Aβ lowering strategy.

It is generally accepted that newly produced Aβ exists in dynamic equilibrium between soluble and deposited forms in the brain, with continual transport of soluble Aβ out of the brain and into the circulation (10). In this regard, it has been reported that TA inhibits Aβ fibrillogenesis, and destabilizes preformed Aβ fibrils *in vitro* (30). We tested the impact of TA on various pools of Aβ peptides *in vivo*, and observed that TA treatment nonselectively reduced Aβ in TBS-, SDS-, and guanidine HCl-soluble brain homogenate fractions from PSAPP mice. One interesting exception was TBS-soluble $A\beta_{1-42}$, which remained unaltered by oral TA treatment. $A\beta_{1-42}$ is typically thought to have a higher propensity to form oligomers and higher molecular weight aggregates than $A\beta_{1-40}$ (11, 74), and we went on to probe whether TA impacted Aβ oligomers. Data showed a reduced abundance of both monomeric and oligomeric Aβ by Western blot and reduced Aβ oligomers by sandwich ELISA in brain homogenates from TA-treated PSAPP mice. These results may be because of a combination of reduced APP metabolism to Aβ (concentration-dependent effect on Aβ oligomer formation) and perhaps a more direct effect of TA on inhibiting assembly of structured Aβ oligomers/aggregates as has been demonstrated for both TA and EGCG (30, 75). If this were the case, then it opens the possibility of a negative feedback loop where loss of Aβ oligomers might down-regulate BACE1 activity and/or expression.

Although our *in vivo* and *in vitro* data suggest that TA has a direct effect on reducing Aβ production by neuronal cells, it remains possible *in vivo* that the compound exerts its effects on non-neuronal cell types as well. For example, TA has been reported to have antioxidant and anti-inflammatory properties (76, 77), and we went on to determine whether the compound impacted neuroinflammation, an important AD pathoetiologic hallmark (53, 54), in PSAPP mice. Interestingly, oral TA treatment reduced microgliosis, astrocytosis, and expression of the proinflammatory cytokines TNF-α and IL-1β in PSAPP mice. One interpretation of these results is that TA has an anti-inflammatory effect independent of its anti-amyloidogenic property. Yet, it is important to note that neuroinflammation and cerebral amyloid generally correlate in mouse models and in human AD (18, 42, 43, 55–57, 78). Thus, it remains possible that reduced neuroinflammation is secondary to TA amelioration of cerebral amyloidosis.

It deserves mentioning that our present findings are given added importance based on the intense β-secretase inhibition focus as an Alzheimer therapeutic approach. Unfortunately, designer drugs have yet to pan out in the clinic, and ~16 compounds have been abandoned by pharmaceutical companies, mainly due to toxicity issues in pre-clinical rodent models of the disease (alzforum.org). The present nutraceutical approach offers a new class of drug for inhibiting β-secretase with few if any side effects in PSAPP mice or in humans, and provides proof-of-concept that BACE1 is indeed still a "drug-able target."

In conclusion, our data demonstrate that the plant-derived polyphenol, TA, opposes behavioral impairment and AD-like pathology in PSAPP mice. These beneficial effects occur with reduction in: cerebral Aβ pathology, cleavage of β-CTF, sAPP-β, BACE1 protein expression and activity, and neuroinflammation. If Aβ pathology in these transgenic models is representative of the clinical syndrome, then our data raise the possibility that dietary supplementation with TA may represent a potentially safe and effective AD prophylaxis.

Acknowledgments—We thank Dr. Joshua J. Breunig for helpful discussion of the manuscript, and Dr. Gopal Thinakaran for generously gifting the SweAPP N2a cells.

REFERENCES

1. Brookmeyer, R., and Gray, S. (2000) Methods for projecting the incidence and prevalence of chronic diseases in aging populations: application to Alzheimer's disease. *Stat. Med.* **19,** 1481–1493
2. Selkoe, D. J. (2001) Alzheimer's disease: genes, proteins, and therapy. *Physiol. Rev.* **81,** 741–766
3. Rozemuller, J. M., Eikelenboom, P., Stam, F. C., Beyreuther, K., and Masters, C. L. (1989) A4 protein in Alzheimer's disease: primary and secondary cellular events in extracellular amyloid deposition. *J. Neuropathol. Exp. Neurol.* **48,** 674–691
4. Hardy, J., and Allsop, D. (1991) Amyloid deposition as the central event in the aetiology of Alzheimer's disease. *Trends Pharmacol. Sci.* **12,** 383–388
5. De Strooper, B., Saftig, P., Craessaerts, K., Vanderstichele, H., Guhde, G., Annaert, W., Von Figura, K., and Van Leuven, F. (1998) Deficiency of presenilin-1 inhibits the normal cleavage of amyloid precursor protein. *Nature* **391,** 387–390
6. Sinha, S., and Lieberburg, I. (1999) Cellular mechanisms of β-amyloid production and secretion. *Proc. Natl. Acad. Sci. U.S.A.* **96,** 11049–11053
7. Vassar, R., Bennett, B. D., Babu-Khan, S., Kahn, S., Mendiaz, E. A., Denis, P., Teplow, D.B., Ross, S., Amarante, P., Loeloff, R., Luo, Y., Fisher, S., Fuller, J., Edenson, S., Lile, J., Jarosinski, M. A., Biere, A. L., Curran, E., Burgess, T., Louis, J. C., Collins, F., Treanor, J., Rogers, G., and Citron, M. (1999) β-Secretase cleavage of Alzheimer's amyloid precursor protein by the transmembrane aspartic protease BACE. *Science* **286,** 735–741
8. Vassar, R., Kovacs, D. M., Yan, R., and Wong, P. C. (2009) The β-secretase enzyme BACE in health and Alzheimer's disease: regulation, cell biology, function, and therapeutic potential. *J. Neurosci.* **29,** 12787–12794
9. Yan, R., Bienkowski, M. J., Shuck, M. E., Miao, H., Tory, M. C., Pauley, A. M., Brashier, J. R., Stratman, N. C., Mathews, W. R., Buhl, A. E., Carter, D. B., Tomasselli, A. G., Parodi, L. A., Heinrikson, R. L., and Gurney, M. E. (1999) Membrane-anchored aspartyl protease with Alzheimer's disease β-secretase activity. *Nature* **402,** 533–537
10. DeMattos, R. B., Bales, K. R., Cummins, D. J., Paul, S. M., and Holtzman, D. M. (2002) Brain to plasma amyloid-β efflux: a measure of brain amyloid burden in a mouse model of Alzheimer's disease. *Science* **295,** 2264–2267
11. Walsh, D. M., Klyubin, I., Fadeeva, J. V., Cullen, W. K., Anwyl, R., Wolfe, M. S., Rowan, M. J., and Selkoe, D. J. (2002) Naturally secreted oligomers of amyloid β protein potently inhibit hippocampal long-term potentiation *in vivo*. *Nature* **416,** 535–539
12. Cleary, J. P., Walsh, D. M., Hofmeister, J. J., Shankar, G. M., Kuskowski, M. A., Selkoe, D. J., and Ashe, K. H. (2005) Natural oligomers of the amyloid-β protein specifically disrupt cognitive function. *Nat. Neurosci.* **8,** 79–84
13. Shankar, G. M., Li, S., Mehta, T. H., Garcia-Munoz, A., Shepardson, N. E., Smith, I., Brett, F. M., Farrell, M. A., Rowan, M. J., Lemere, C. A., Regan, C. M., Walsh, D. M., Sabatini, B. L., and Selkoe, D. J. (2008) Amyloid-β protein dimers isolated directly from Alzheimer's brains impair synaptic plasticity and memory. *Nat. Med.* **14,** 837–842
14. Schenk, D., Barbour, R., Dunn, W., Gordon, G., Grajeda, H., Guido, T., Hu, K., Huang, J., Johnson-Wood, K., Khan, K., Kholodenko, D., Lee, M., Liao, Z., Lieberburg, I., Motter, R., Mutter, L., Soriano, F., Shopp, G., Vasquez,

N., Vandevert, C., Walker, S., Wogulis, M., Yednock, T., Games, D., and Seubert, P. (1999) Immunization with amyloid-β attenuates Alzheimer-disease-like pathology in the PDAPP mouse. *Nature* **400,** 173–177
15. Weggen, S., Eriksen, J. L., Das, P., Sagi, S. A., Wang, R., Pietrzik, C. U., Findlay, K. A., Smith, T. E., Murphy, M. P., Bulter, T., Kang, D. E., Marquez-Sterling, N., Golde, T. E., and Koo, E. H. (2001) A subset of NSAIDs lower amyloidogenic Aβ42 independently of cyclooxygenase activity. *Nature* **414,** 212–216
16. Tan, J., Town, T., Crawford, F., Mori, T., DelleDonne, A., Crescentini, R., Obregon, D., Flavell, R. A., and Mullan, M. J. (2002) Role of CD40 ligand in amyloidosis in transgenic Alzheimer's mice. *Nat. Neurosci.* **5,** 1288–1293
17. Kukar, T. L., Ladd, T. B., Bann, M. A., Fraering, P. C., Narlawar, R., Maharvi, G. M., Healy, B., Chapman, R., Welzel, A. T., Price, R. W., Moore, B., Rangachari, V., Cusack, B., Eriksen, J., Jansen-West, K., Verbeeck, C., Yager, D., Eckman, C., Ye, W., Sagi, S., Cottrell, B. A., Torpey, J., Rosenberry, T. L., Fauq, A., Wolfe, M. S., Schmidt, B., Walsh, D. M., Koo, E. H., and Golde, T. E. (2008) Substrate-targeting γ-secretase modulators. *Nature* **453,** 925–929
18. Town, T., Laouar, Y., Pittenger, C., Mori, T., Szekely, C.A., Tan, J., Duman, R. S., and Flavell, R. A. (2008) Blocking TGF-β-Smad2/3 innate immune signaling mitigates Alzheimer-like pathology. *Nat. Med.* **14,** 681–687
19. Zhu, Y., Hou, H., Rezai-Zadeh, K., Giunta, B., Ruscin, A., Gemma, C., Jin, J., Dragicevic, N., Bradshaw, P., Rasool, S., Glabe, C. G., Ehrhart, J., Bickford, P., Mori, T., Obregon, D., Town, T., and Tan, J. (2011) CD45 deficiency drives amyloid-β peptide oligomers and neuronal loss in Alzheimer's disease mice. *J. Neurosci.* **31,** 1355–1365
20. Breitner, J., Evans, D., Lyketsos, C., Martin, B., and Meinert, C. (2007) ADAPT trial data. *Am. J. Med.* **120,** e3
21. Montine, T. J., Sonnen, J. A., Milne, G., Baker, L. D., and Breitner, J. C. (2010) Elevated ratio of urinary metabolites of thromboxane and prostacyclin is associated with adverse cardiovascular events in ADAPT. *PLoS One* **5,** e9340
22. Georgiou, N. A., Garssen, J., and Witkamp, R. F. (2011) Pharma-nutrition interface: the gap is narrowing. *Eur. J. Pharmacol.* **651,** 1–8
23. Rezai-Zadeh, K., Shytle, D., Sun, N., Mori, T., Hou, H., Jeanniton, D., Ehrhart, J., Townsend, K., Zeng, J., Morgan, D., Hardy, J., Town, T., and Tan, J. (2005) Green tea epigallocatechin-3-gallate (EGCG) modulates amyloid precursor protein cleavage and reduces cerebral amyloidosis in Alzheimer transgenic mice. *J. Neurosci.* **25,** 8807–8814
24. Obregon, D. F., Rezai-Zadeh, K., Bai, Y., Sun, N., Hou, H., Ehrhart, J., Zeng, J., Mori, T., Arendash, G. W., Shytle, D., Town, T., and Tan, J. (2006) ADAM10 activation is required for green tea (−)-epigallocatechin-3-gallate-induced α-secretase cleavage of amyloid precursor protein. *J. Biol. Chem.* **281,** 16419–16427
25. Rezai-Zadeh, K., Douglas Shytle, R., Bai, Y., Tian, J., Hou, H., Mori, T., Zeng, J., Obregon, D., Town, T., and Tan, J. (2009) Flavonoid-mediated presenilin-1 phosphorylation reduces Alzheimer's disease β-amyloid production. *J. Cell Mol. Med.* **13,** 574–588
26. Ono, K., Yoshiike, Y., Takashima, A., Hasegawa, K., Naiki, H., and Yamada, M. (2003) Potent anti-amyloidogenic and fibril-destabilizing effects of polyphenols *in vitro*: implications for the prevention and therapeutics of Alzheimer's disease. *J. Neurochem.* **87,** 172–181
27. Marambaud, P., Zhao, H., and Davies, P. (2005) Resveratrol promotes clearance of Alzheimer's disease amyloid-β peptides. *J. Biol. Chem.* **280,** 37377–37382
28. Arendash, G. W., Mori, T., Cao, C., Mamcarz, M., Runfeldt, M., Dickson, A., Rezai-Zadeh, K., Tan, J., Citron, B. A., Lin, X., Echeverria, V., and Potter, H. (2009) Caffeine reverses cognitive impairment and decreases brain amyloid-β levels in aged Alzheimer's disease mice. *J. Alzheimers Dis.* **17,** 661–680
29. Serrano, J., Puupponen-Pimiä, R., Dauer, A., Aura, A. M., and Saura-Calixto, F. (2009) Tannins: current knowledge of food sources, intake, bioavailability and biological effects. *Mol. Nutr. Food Res.* **53,** S310–S329
30. Ono, K., Hasegawa, K., Naiki, H., and Yamada, M. (2004) Anti-amyloidogenic activity of tannic acid and its activity to destabilize Alzheimer's β-amyloid fibrils *in vitro*. *Biochim. Biophys. Acta* **1690,** 193–202
31. Ehrnhoefer, D. E., Bieschke, J., Boeddrich, A., Herbst, M., Masino, L., Lurz, R., Engemann, S., Pastore, A., and Wanker, E. E. (2008) EGCG redirects amyloidogenic polypeptides into unstructured, off-pathway oligomers. *Nat. Struct. Mol. Biol.* **15,** 558–566
32. Meng, F., Abedini, A., Plesner, A., Verchere, C. B., and Raleigh, D. P. (2010) The flavanol (−)-epigallocatechin 3-gallate inhibits amyloid formation by islet amyloid polypeptide, disaggregates amyloid fibrils, and protects cultured cells against IAPP-induced toxicity. *Biochemistry* **49,** 8127–8133
33. Borchelt, D. R., Ratovitski, T., van Lare, J., Lee, M. K., Gonzales, V., Jenkins, N. A., Copeland, N. G., Price, D. L., and Sisodia, S. S. (1997) Accelerated amyloid deposition in the brains of transgenic mice coexpressing mutant presenilin 1 and amyloid precursor proteins. *Neuron* **19,** 939–945
34. Arendash, G. W., King, D. L., Gordon, M. N., Morgan, D., Hatcher, J. M., Hope, C. E., and Diamond, D. M. (2001) Progressive, age-related behavioral impairments in transgenic mice carrying both mutant amyloid precursor protein and presenilin-1 transgenes. *Brain Res.* **891,** 42–53
35. Jankowsky, J. L., Slunt, H. H., Gonzales, V., Jenkins, N. A., Copeland, N. G., and Borchelt, D. R. (2004) APP processing and amyloid deposition in mice haplo-insufficient for presenilin 1. *Neurobiol. Aging* **25,** 885–892
36. Garcia-Alloza, M., Robbins, E. M., Zhang-Nunes, S. X., Purcell, S. M., Betensky, R. A., Raju, S., Prada, C., Greenberg, S. M., Bacskai, B. J., and Frosch, M. P. (2006) Characterization of amyloid deposition in the APPswe/PS1dE9 mouse model of Alzheimer disease. *Neurobiol. Dis.* **24,** 516–524
37. Laghmouch, A., Bertholet, J. Y., and Crusio, W. E. (1997) Hippocampal morphology and open-field behavior in *Mus musculus domesticus* and *Mus spretus* inbred mice. *Behav. Genet.* **27,** 67–73
38. Kim, K. S., and Han, P. L. (2006) Optimization of chronic stress paradigms using anxiety- and depression-like behavioral parameters. *J. Neurosci. Res.* **83,** 497–507
39. De Rosa, R., Garcia, A. A., Braschi, C., Capsoni, S., Maffei, L., Berardi, N., and Cattaneo, A. (2005) Intranasal administration of nerve growth factor (NGF) rescues recognition memory deficits in AD11 anti-NGF transgenic mice. *Proc. Natl. Acad. Sci. U.S.A.* **102,** 3811–3816
40. Morris, R.G., Garrud, P., Rawlins, J. N., and O'Keefe, J. (1982) Place navigation impaired in rats with hippocampal lesions. *Nature* **297,** 681–683
41. Good, M., and Honey, R. C. (1997) Dissociable effects of selective lesions to hippocampal subsystems on exploratory behavior, contextual learning, and spatial learning. *Behav. Neurosci.* **111,** 487–493
42. Mori, T., Town, T., Tan, J., Yada, N., Horikoshi, Y., Yamamoto, J., Shimoda, T., Kamanaka, Y., Tateishi, N., and Asano, T. (2006) Arundic acid ameliorates cerebral amyloidosis and gliosis in Alzheimer transgenic mice. *J. Pharmacol. Exp. Ther.* **318,** 571–578
43. Mori, T., Koyama, N., Arendash, G. W., Horikoshi-Sakuraba, Y., Tan, J., and Town, T. (2010) Overexpression of human S100B exacerbates cerebral amyloidosis and gliosis in the Tg2576 mouse model of Alzheimer's disease. *Glia* **58,** 300–314
44. Franklin, K. B. J., and Paxinos, G. (2001) *The Mouse Brain in Stereotaxic Coordinates*, Academic Press, San Diego, CA
45. Tan, J., Town, T., Mori, T., Wu, Y., Saxe, M., Crawford, F., and Mullan, M. (2000) CD45 opposes β-amyloid peptide-induced microglial activation via inhibition of p44/42 mitogen-activated protein kinase. *J. Neurosci.* **20,** 7587–7594
46. Kawarabayashi, T., Younkin, L. H., Saido, T. C., Shoji, M., Ashe, K. H., and Younkin, S. G. (2001) Age-dependent changes in brain, CSF, and plasma amyloid β protein in the Tg2576 transgenic mouse model of Alzheimer's disease. *J. Neurosci.* **21,** 372–381
47. Jankowsky, J. L., Slunt, H. H., Gonzales, V., Savonenko, A. V., Wen, J. C., Jenkins, N. A., Copeland, N. G., Younkin, L. H., Lester, H. A., Younkin, S. G., and Borchelt, D. R. (2005) Persistent amyloidosis following suppression of Aβ production in a transgenic model of Alzheimer disease. *PLoS Med.* **2,** e355
48. Horikoshi, Y., Sakaguchi, G., Becker, A. G., Gray, A. J., Duff, K., Aisen, P. S., Yamaguchi, H., Maeda, M., Kinoshita, N., and Matsuoka, Y. (2004) Development of Aβ terminal end-specific antibodies and sensitive ELISA for Aβ variant. *Biochem. Biophys. Res. Commun.* **319,** 733–737
49. Xia, W., Yang, T., Shankar, G., Smith, I. M., Shen, Y., Walsh, D. M., and Selkoe, D. J. (2009) A specific enzyme-linked immunosorbent assay for measuring β-amyloid protein oligomers in human plasma and brain tissue of patients with Alzheimer disease. *Arch. Neurol.* **66,** 190–199

50. Monney, L., Sabatos, C. A., Gaglia, J. L., Ryu, A., Waldner, H., Chernova, T., Manning, S., Greenfield, E. A., Coyle, A. J., Sobel, R. A., Freeman, G. J., and Kuchroo, V. K. (2002) Th1-specific cell surface protein Tim-3 regulates macrophage activation and severity of an autoimmune disease. *Nature* **415,** 536–541
51. King, D. L., Arendash, G. W., Crawford, F., Sterk, T., Menendez, J., and Mullan, M. J. (1999) Progressive and gender-dependent cognitive impairment in the APP_{sw} transgenic mouse model for Alzheimer's disease. *Behav. Brain Res.* **103,** 145–162
52. Ellis, R. J., Olichney, J. M., Thal, L. J., Mirra, S. S., Morris, J. C., Beekly, D., and Heyman, A. (1996) Cerebral amyloid angiopathy in the brains of patients with Alzheimer's disease: the CERAD experience, Part XV. *Neurology* **46,** 1592–1596
53. Griffin, W. S., Sheng, J. G., Royston, M. C., Gentleman, S. M., McKenzie, J. E., Graham, D. I., Roberts, G. W., and Mrak, R. E. (1998) Glial-neuronal interactions in Alzheimer's disease: the potential role of a 'cytokine cycle' in disease progression. *Brain Pathol.* **8,** 65–72
54. Akiyama, H., Barger, S., Barnum, S., Bradt, B., Bauer, J., Cole, G. M., Cooper, N. R., Eikelenboom, P., Emmerling, M., Fiebich, B. L., Finch, C. E., Frautschy, S., Griffin, W. S., Hampel, H., Hull, M., Landreth, G., Lue, L., Mrak, R., Mackenzie, I. R., McGeer, P. L., O'Banion, M. K., Pachter, J., Pasinetti, G., Plata-Salaman, C., Rogers, J., Rydel, R., Shen, Y., Streit, W., Strohmeyer, R., Tooyoma, I., Van Muiswinkel, F. L., Veerhuis, R., Walker, D., Webster, S., Wegrzyniak, B., Wenk, G., and Wyss-Coray, T. (2000) Inflammation and Alzheimer's disease. *Neurobiol. Aging* **21,** 383–421
55. Benzing, W. C., Wujek, J. R., Ward, E. K., Shaffer, D., Ashe, K. H., Younkin, S. G., and Brunden, K. R. (1999) Evidence for glial-mediated inflammation in aged APP_{sw} transgenic mice. *Neurobiol. Aging* **20,** 581–589
56. Stalder, M., Phinney, A., Probst, A., Sommer, B., Staufenbiel, M., and Jucker, M. (1999) Association of microglia with amyloid plaques in brains of APP23 transgenic mice. *Am. J. Pathol.* **154,** 1673–1684
57. Lim, G. P., Yang, F., Chu, T., Chen, P., Beech, W., Teter, B., Tran, T., Ubeda, O., Ashe, K. H., Frautschy, S. A., and Cole, G. M. (2000) Ibuprofen suppresses plaque pathology and inflammation in a mouse model for Alzheimer's disease. *J. Neurosci.* **20,** 5709–5714
58. Stalder, A. K., Ermini, F., Bondolfi, L., Krenger, W., Burbach, G. J., Deller, T., Coomaraswamy, J., Staufenbiel, M., Landmann, R., and Jucker, M. (2005) Invasion of hematopoietic cells into the brain of amyloid precursor protein transgenic mice. *J. Neurosci.* **25,** 11125–11132
59. Ito, D., Tanaka, K., Suzuki, S., Dembo, T., and Fukuuchi, Y. (2001) Enhanced expression of Iba1, ionized calcium-binding adapter molecule 1, after transient focal cerebral ischemia in rat brain. *Stroke* **32,** 1208–1215
60. Streit, W. J. (2005) in *Neuroglia* (Kettermann, H., and Ransom, B. R., eds) pp. 60–71, Oxford University Press, New York
61. Nepka, C., Sivridis, E., Antonoglou, O., Kortsaris, A., Georgellis, A., Taitzoglou, I., Hytiroglou, P., Papadimitriou, C., Zintzaras, I., and Kouretas, D. (1999) Chemopreventive activity of very low dose dietary tannic acid administration in hepatoma bearing C3H male mice. *Cancer Lett.* **141,** 57–62
62. Chen, S. C., and Chung, K. T. (2000) Mutagenicity and antimutagenicity studies of tannic acid and its related compounds. *Food Chem. Toxicol.* **38,** 1–5
63. Andrade, R. G., Jr., Dalvi, L. T., Silva, J. M., Jr., Lopes, G. K., Alonso, A., and Hermes-Lima, M. (2005) The antioxidant effect of tannic acid on the *in vitro* copper-mediated formation of free radicals. *Arch. Biochem. Biophys.* **437,** 1–9
64. Zhang, H., Zhu, S. J., Wang, D., Wei, Y. J., and Hu, S. S. (2009) Intramyocardial injection of tannic acid attenuates postinfarction remodeling: a novel approach to stabilize the breaking extracellular matrix. *J. Thorac. Cardiovasc. Surg.* **137,** 216–222, 222e1–2
65. Yokozawa, T., Fujioka, K., Oura, H., Nonaka, G., and Nishioka, I. (1991) Effects of rhubarb tannins on uremic toxins. *Nephron* **58,** 155–160
66. Boyd, E. M., Bereczky, K., and Godi, I. (1965) The acute toxicity of tannic acid administered intragastrically. *Can. Med. Assoc. J.* **92,** 1292–1297
67. Bian, Y., Masuda, A., Matsuura, T., Ito, M., Okushin, K., Engel, A. G., and Ohno, K. (2009) Tannic acid facilitates expression of the polypyrimidine tract binding protein and alleviates deleterious inclusion of CHRNA1 exon P3A due to an hnRNP H-disrupting mutation in congenital myasthenic syndrome. *Hum. Mol. Genet.* **18,** 1229–1237
68. Medić-Sarić, M., Rastija, V., Bojić, M., and Males, Z. (2009) From functional food to medicinal product: systematic approach in analysis of polyphenolics from propolis and wine. *Nutr. J.* **8,** 33
69. Konishi, Y., Hitomi, Y., and Yoshioka, E. (2004) Intestinal absorption of *p*-coumaric and gallic acids in rats after oral administration. *J. Agric. Food Chem.* **52,** 2527–2532
70. Shahrzad, S., Aoyagi, K., Winter, A., Koyama, A., and Bitsch, I. (2001) Pharmacokinetics of gallic acid and its relative bioavailability from tea in healthy humans. *J. Nutr.* **131,** 1207–1210
71. Mandel, S., Amit, T., Reznichenko, L., Weinreb, O., and Youdim, M. B. (2006) Green tea catechins as brain-permeable, natural iron chelators-antioxidants for the treatment of neurodegenerative disorders. *Mol. Nutr. Food Res.* **50,** 229–234
72. Ferruzzi, M. G., Lobo, J. K., Janle, E. M., Cooper, B., Simon, J. E., Wu, Q. L., Welch, C., Ho, L., Weaver, C., and Pasinetti, G. M. (2009) Bioavailability of gallic acid and catechins from grape seed polyphenol extract is improved by repeated dosing in rats: implications for treatment in Alzheimer's disease. *J. Alzheimers's Dis.* **18,** 113–124
73. Gandhi, S., Refolo, L. M., and Sambamurti, K. (2004) Amyloid precursor protein compartmentalization restricts β-amyloid production: therapeutic targets based on BACE compartmentalization. *J. Mol. Neurosci.* **24,** 137–143
74. Lesné, S., Koh, M. T., Kotilinek, L., Kayed, R., Glabe, C. G., Yang, A., Gallagher, M., and Ashe, K.H. (2006) A specific amyloid-β protein assembly in the brain impairs memory. *Nature* **440,** 352–357
75. Bieschke, J., Russ, J., Friedrich, R. P., Ehrnhoefer, D.E., Wobst, H., Neugebauer, K., and Wanker, E. E. (2010) EGCG remodels mature α-synuclein and amyloid-β fibrils and reduces cellular toxicity. *Proc. Natl. Acad. Sci. U.S.A.* **107,** 7710–7715
76. Gali, H. U., Perchellet, E. M., Klish, D. S., Johnson, J. M., and Perchellet, J. P. (1992) Hydrolyzable tannins: potent inhibitors of hydroperoxide production and tumor promotion in mouse skin treated with 12-*O*-tetradecanoylphorbol-13-acetate *in vivo*. *Int. J. Cancer* **51,** 425–432
77. Sehrawat, A., Sharma, S., and Sultana, S. (2006) Preventive effect of tannic acid on 2-acetylaminofluorene induced antioxidant level, tumor promotion and hepatotoxicity: a chemopreventive study. *Redox Rep.* **11,** 85–95
78. McGeer, P. L., Itagaki, S., Tago, H., and McGeer, E. G. (1987) Reactive microglia in patients with senile dementia of the Alzheimer type are positive for the histocompatibility glycoprotein HLA-DR. *Neurosci. Lett.* **79,** 195–200

Journal of Cellular and Molecular Medicine
A JOURNAL OF TRANSLATIONAL MEDICINE

J. Cell. Mol. Med. Vol 16, No 2, 2012 pp. 287-295

High-molecular weight Aβ oligomers and protofibrils are the predominant Aβ species in the native soluble protein fraction of the AD brain

Ajeet Rijal Upadhaya [a], Irina Lungrin [a, b], Haruyasu Yamaguchi [c], Marcus Fändrich [d], Dietmar Rudolf Thal [a, *]

[a] *Laboratory of Neuropathology-Institute of Pathology, Center for Clinical Research at the University of Ulm, Ulm, Germany*
[b] *Department of Neurology, Center for Clinical Research at the University of Ulm, Ulm, Germany*
[c] *Gunma University of Health Sciences, Maebashi, Gunma, Japan*
[d] *Max Planck Research Unit for Enzymology of Protein Folding and Martin-Luther University Halle-Wittenberg, Halle an der Saale, Germany*

Received: November 3, 2010; Accepted: March 7, 2011

Abstract

Alzheimer's disease (AD) is characterized by the aggregation and deposition of amyloid β protein (Aβ) in the brain. Soluble Aβ oligomers are thought to be toxic. To investigate the predominant species of Aβ protein that may play a role in AD pathogenesis, we performed biochemical analysis of AD and control brains. Sucrose buffer-soluble brain lysates were characterized in native form using blue native (BN)-PAGE and also in denatured form using SDS-PAGE followed by Western blot analysis. BN-PAGE analysis revealed a high-molecular weight smear (>1000 kD) of $Aβ_{42}$-positive material in the AD brain, whereas low-molecular weight and monomeric Aβ species were not detected. SDS-PAGE analysis, on the other hand, allowed the detection of prominent Aβ monomer and dimer bands in AD cases but not in controls. Immunoelectron microscopy of immunoprecipitated oligomers and protofibrils/fibrils showed spherical and protofibrillar Aβ-positive material, thereby confirming the presence of high-molecular weight Aβ (hiMWAβ) aggregates in the AD brain. *In vitro* analysis of synthetic $Aβ_{40}$- and $Aβ_{42}$ preparations revealed Aβ fibrils, protofibrils, and hiMWAβ oligomers that were detectable at the electron microscopic level and after BN-PAGE. Further, BN-PAGE analysis exhibited a monomer band and less prominent low-molecular weight Aβ (loMWAβ) oligomers. In contrast, SDS-PAGE showed large amounts of loMWAβ but no hiMWA$β_{40}$ and strikingly reduced levels of hiMWA$β_{42}$. These results indicate that hiMWAβ aggregates, particularly $Aβ_{42}$ species, are most prevalent in the soluble fraction of the AD brain. Thus, soluble hiMWAβ aggregates may play an important role in the pathogenesis of AD either independently or as a reservoir for release of loMWAβ oligomers.

Keywords: amyloid β protein • protofibrils • fibrils • oligomers • Alzheimer's disease

Introduction

Alzheimer's disease (AD) is characterized by the extracellular deposition of amyloid β protein (Aβ) aggregates in the brain [1]. Although high-molecular weight Aβ (hiMWAβ) oligomers, Aβ protofibrils and fibrils, low-molecular weight Aβ (loMWAβ) oligomers, such as dimers, trimers or Aβ*56, have been observed in human AD brain tissue or in mouse models of AD [1–9], it is not entirely clear which Aβ species are the most relevant ones for the development of AD and how these Aβ forms are related to one another *in vivo*. Some studies have used SDS-PAGE for protein analysis [3–5, 9], which denatures and dissociates proteins into individual polypeptides before determining its molecular weight. By contrast, others have performed only dot blot analysis [6]. Currently, only size exclusion chromatography has been used to study oligomers in non-SDS-treated conditions [3, 9]. However, it

*Correspondence to: Dietmar R. THAL,
Laboratory of Neuropathology-Institute of Pathology,
Center for Clinical Research at the University of Ulm,
Helmholtzstrasse 8/1, D-89081 Ulm, Germany.
Tel.: +49-8221-96-2163
Fax: +49-8221-96-28158
E-mail: Dietmar.Thal@uni-ulm.de

doi:10.1111/j.1582-4934.2011.01306.x

is unclear whether interactions with the stationary phase may impact the aggregation state of hiMWAβ species. A detailed analysis of the native Aβ aggregates in the AD brain using blue native-PAGE (BN-PAGE) in comparison with SDS-PAGE analysis that focuses on the identification of the above-mentioned forms of Aβ aggregates is still unavailable.

Antibodies and antibody fragments have been developed to detect specific hiMWAβ oligomers (A11) and protofibrillar/fibrillar conformations (B10AP) [2, 6]. These antibodies and antibody fragments allow isolation of oligomers, protofibrils and fibrils from soluble native protein lysates by immunoprecipitation for further protein analysis. Here, we employed these antibodies and BN-PAGE analysis to clarify whether soluble hiMWAβ oligomers and Aβ protofibrils/fibrils or Aβ dimers and other loMWAβ species represent the predominant Aβ aggregates in the native soluble fraction of the AD brain. SDS-PAGE was used to study the effect of protein denaturation on the spectrum of loMWAβ and hiMWAβ species.

Materials and methods

Neuropathology and human sample characterization

A sample including six AD and four control cases was studied (Table 1). All autopsy brains were collected from individuals who died in the University Hospitals of Bonn or Ulm (Germany). All human tissue was obtained and processed in compliance with German federal laws and with university ethics committee approval.

Demented as well as non-demented patients were examined 1–4 weeks prior to death using standardized protocols for routine clinical examination, including neurological status, upon admission to hospital. These data were used to determine whether individuals clinically fulfilled the DSM-IV criteria for dementia [11]. AD was diagnosed when dementia was observed and when the degree of AD-related neuropathology indicated at least a moderate likelihood for AD according to internationally acknowledged criteria [12].

After assessment of unfixed tissue from one hemisphere for biochemical studies, the brains were fixed in a 4% aqueous formaldehyde solution for at least 3 weeks before undergoing neuropathological screening. Presence or absence of gross infarction, haemorrhage, tumour and other findings were recorded. Tissue blocks from the medial temporal lobe (MTL) were excised at the levels of the (*i*) anterior limit of the dentate gyrus and (*ii*) lateral geniculate body [13]. These blocks together with tissue blocks from the occipital cortex (Brodmann areas 17–19) were embedded in paraffin. All sections were cut at 10 μm.

Neurofibrillary changes were detected by immunostaining with an antibody directed against abnormal phosphorylated τ protein (AT-8, Pierce, Rockford, IL, USA, 1/1000) [14]. Neuritic plaques were also diagnosed in sections immunostained with this same antibody. The presence of Aβ deposition was assessed using immunohistochemistry with an antibody raised against $Aβ_{17–24}$ (4G8 [15], Covance, Emeryville, CA, USA, 1/5000, formic acid pre-treatment).

Diagnosis of the stages in the development of neurofibrillary changes (Braak NFT stage) and the semi-quantitative assessment of neuritic plaques (CERAD score) were performed in accordance with published and recommended criteria [12, 14, 16, 17]. For staging of Aβ pathology, we used a previously published protocol for four phases of β-amyloidosis in the MTL [18]. This hierarchically based procedure facilitates study of the topographic distribution pattern of Aβ deposition in additional brain regions [18, 19]: phase 1 represents Aβ deposition that is restricted to the temporal neocortex. Phase 2 is characterized by the presence of additional Aβ plaques in the entorhinal cortex and/or in the hippocampal subiculum-CA1 region. The third phase is marked by the presence of Aβ plaques in the outer zone of the molecular layer of the fascia dentata, subpial band-like amyloid and/or presubicular 'lake-like' amyloid. The existence of further Aβ plaques in the hippocampal sector CA4 and/or the pre-α layer of the entorhinal cortex characterize the fourth and final phase of Aβ deposition in the MTL. Reference pathology for all cases was performed by one and the same neuropathologist (D.R.T.).

Table 1 List of autopsy cases studied

Case no.	Diagnosis	Age	Gender	AD type	Braak-NFT stage	Aβ phase	CERAD plaque score
1	Control	60	m	0	0	0	0
2	Control	66	m	0	I	0	0
3	Control	69	f	0	I	0	0
4	Control	71	f	0	I	0	0
5	AD	79	f	1	IV	3	2
6	AD	78	m	1	IV	4	1
7	AD	62	f	1	VI	4	3
8	AD	91	f	2	IV	3	1
9	AD	84	m	2	VI	4	3
10	AD	64	f	2	VI	4	3

Ten autopsy cases (four controls, including two females and two males, age range 60–71 years; mean age ± S.D.: 66.5 ± 4.8 years and six AD cases, including four females and two males, age range 62–91 years; mean age ± S.D.: 76.3 ± 11.33 years) were analysed. The table shows neuropathological diagnosis of AD according to published criteria [12], age in years, gender, AD type [10], the stage of neurofibrillary tangle (Braak-NFT stage) pathology according to Braak *et al.* [14, 16], the Aβ-phase representing the distribution of Aβ deposits in subfields of the MTL [18] and the Consortium to Establish a Registry for Alzheimer's Disease (CERAD) score for the frequency of neuritic plaques according to Mirra *et al.* [17]. m: male; f: female; AD: Alzheimer's disease.

Biochemical analysis of human AD and control brains

Fresh frozen human brain tissue from the six AD and four control cases was used to assess the presence and types of native Aβ aggregates in AD and control brains (Table 1). Protein extraction from 30 mg of fresh frozen human occipital (Brodmann areas 17–19) and temporal cortex (Brodmann

areas 35 and 36) was carried out in 2 ml of 0.32 M sucrose dissolved in 1 M Tris-buffer (pH 7.4) with a protease and phosphatase inhibitor cocktail (Complete and PhosSTOP, Roche, Mannheim, Germany). The tissue was homogenized as previously described [20]. The homogenate was placed on ice for 30 min., and the supernatant was clarified by centrifuging for 30 min. at 14,000 × *g* at 4°C. To avoid the segregation of high-molecular weight proteins from the soluble into the insoluble fraction, a centrifuging speed in excess of 14,000 × *g* was not used. The resultant supernatant, *i.e.* the sucrose-soluble fraction, was aliquoted into appropriate volumes and stored at –80°C until use. Protein amounts were determined using BCA Protein Assay (Bio-Rad, Hercules, CA, USA).

For immunoprecipitation, 200 μl of brain lysate was incubated with 1 μl anti-$A\beta_{1-17}$ (6E10, 1 mg/ml; Covance, Dedham, MA, USA), with 20 μl B10AP antibody fragments coupled to alkaline phosphatase ([2], 0.55 mg/ml) or with 1 μl A11 ([6], 1 mg/ml; Millipore, Temecula, CA, USA) antibodies at 4°C for 4 hrs with gentle agitation. A total of 50 μl of protein G Microbeads (Miltenyi Biotec, Bergisch-Gladbach, Germany) were added to the mixture and incubated overnight at 4°C on a shaking table with gentle agitation. The mixture was then passed through the μColumns which separate the microbeads by retaining them into the column, while the rest of the lysate flows through. After several mild rinsing steps with 1× tris-buffered saline (TBS) buffer (pH 7.4), the microbead-bound proteins were eluted with 1× Lithium dodecyl sulfate (LDS) sample buffer at 95°C (Invitrogen, Carlsbad, CA, USA).

For BN-PAGE of the sucrose fraction, 50 μg of total protein was prepared with 4× NativePAGE sample buffer (Invitrogen) and subjected to native PAGE 4–16% Bis-Tris gel electrophoresis according to the manufacturer's protocol (Invitrogen). Native-Mark unstained protein standards (Invitrogen) were used as molecular weight markers. The gel was equilibrated in transfer buffer containing 0.2% SDS for 10 min. After protein transfer onto the nitrocellulose membranes (Bio-Rad), the membrane was boiled in phosphate-buffered saline (PBS) buffer in microwave oven for 6 min. Washing buffer and antibody dilution buffer contained 1 M PBS (pH 7.4) with 0.02% Tween (BioRad). A total of 3% non-fat dry milk (Roth, Karlsruhe, Germany) diluted in antibody-dilution buffer was used to block unspecific binding for 1 hr at room temperature.

For SDS-PAGE, sucrose fractions (50 μg total protein) and immunoprecipitation products were electrophoretically resolved in a precast NuPAGE 4–12% Bis-Tris gel system (Invitrogen). The protein load was controlled either by Ponceau S staining or β-actin (C4, 1/1000; Santa Cruz Biotechnology, Santa Cruz, CA, USA) immunoblotting. The proteins were transferred to nitrocellulose membranes and the membranes were boiled with PBS for 6 min. followed by blocking with 5% non-fat dry milk (Roth; diluted in antibody-dilution buffer) for 1 hr at room temperature.

For immunodetection of the blotted proteins, the membranes were incubated for 24 hrs at 4°C with the primary antibodies: anti-$A\beta_{1-17}$ (6E10, 1/1000), anti-$A\beta_{42}$ (MBC-42, [21] 1/500), anti-$A\beta_{40}$ (MBC-40, [21] 1/1000) and anti-amyloid precursor protein (APP) (22C11, 1/500; Millipore). The 22C11 anti-APP antibody is directed against an N-terminal part of the APP molecule outside the Aβ region [22]. After washing steps, the corresponding secondary antibodies (EIA grade affinity purified goat antimouse/rabbit IgG-HRP, 1/20000; Bio-Rad) were applied for 2 hrs at room temperature. Blots were developed with an enhanced chemiluminescence (ECL) detection system (Supersignal Pico Western system, ThermoScientific-Pierce, Waltham, MA, USA) and illuminated in ECL Hyperfilm (GE Healthcare, Buckinghamshire, UK). $A\beta_{42}$- and $A\beta_{40}$ preparations were used as positive and/or negative controls. All BN-PAGE blots were developed with standard chemiluminescence exposure time of 2–5 min. up to maximum exposure times of 2–3 hrs to detect even minimal amounts of Aβ aggregates. For SDS-PAGE blots, exposure time of 2–5 min. was used except when otherwise indicated.

Electron microscopy of immunoprecipitated oligomeric and fibrillar/protofibrillar proteins from human AD and control brains

For electron microscopy, 5 μl of immunoprecipitated and redissolved A11-positive oligomers or B10AP-positive protofibrils/fibrils were placed on formvar-coated grids. After 1 min. incubation, the excess liquid was wiped off and the grid dried. The grid then was treated with Na-Borhydrite (0.1% in water for 1 min.) followed by blocking with 5% bovine serum albumin, 5% normal goat serum and 0.1% cold-washed fish gelatin in 1 M PBS. The grids were incubated with anti-$A\beta_{1-17}$ (6E10, 1/50) for 30 min. After washing, the primary antibody was visualized by 15 nm gold-labelled secondary antibodies (1/30, diluted in 1 M PBS; Aurion Immuno Gold Reagents & Accessories, Wageningen, The Netherlands). Then, the grid was post-fixed in 2% glutaraldehyde and block-stained with a 2% aqueous solution of uranyl acetate (Merck, Darmstadt, Germany) for 1 min. followed by five rinsing steps in H_2O_2. The sections were viewed with a Philips EM400T 120KV (Eindhoven, The Netherlands) and with a Zeiss EM10 (Oberkochen, Germany).

Analysis of synthetic $A\beta_{42}$ and $A\beta_{40}$ aggregates in native state and after SDS denaturation

To determine whether synthetic Aβ aggregates primarily form loMWAβ- and hiMWAβ aggregates, we dissolved 15 μmol synthetic $A\beta_{40}$-peptide (Peptides International, Louisville, KY, USA) in 1 ml cell culture medium (Quantum 263; PAA Laboratories, Pasching, Austria) for 30 min. at 4°C [23]. $A\beta_{42}$-peptide (Bachem, Bubendorf, Switzerland) was also dissolved in cell culture medium (RPMI1640; GIBCO, Invitrogen) [23]. Aggregation was permitted to occur for 4 hrs at 22°C. To identify oligomers, fibrils and protofibrils structurally we used electron microscopy. For this purpose, 5 μl of the $A\beta_{40}$- and $A\beta_{42}$ solutions were placed on a formvar-coated grid for 1 min. before wiping off the excess liquid. The protein-coated grids were block-stained with a 2% aqueous solution of uranyl acetate (Merck).

The protein aggregates were also analysed with BN-PAGE and SDS-PAGE as well as subsequent Western blot analysis using the MBC-40 and MBC-42 antibodies to detect $A\beta_{40}$ and $A\beta_{42}$, respectively. This experiment was repeated five times.

Results

High-molecular weight $A\beta_{42}$ aggregates predominate in native protein preparations of the soluble fraction from human brain lysates

BN-PAGE with subsequent Western blot analysis of the soluble fraction of human AD brain lysates revealed a high-molecular weight anti-$A\beta_{42}$-positive smear >1000 kD in AD cases (Fig. 1A)

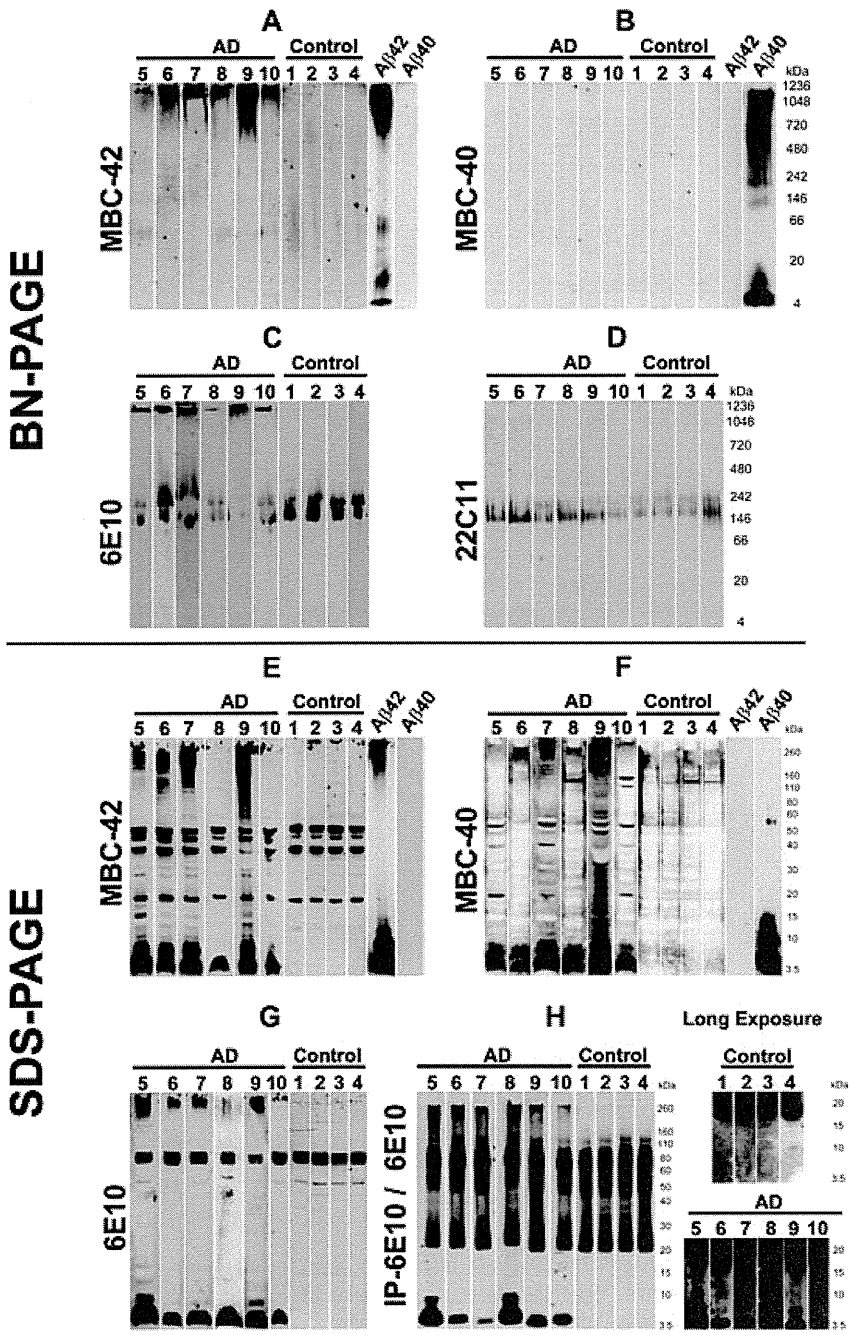

Fig. 1 Western blot analysis of sucrose soluble proteins from AD and control brains after BN-PAGE (**A–D**) and after SDS-PAGE (**E–H**). All BN-PAGE blots were developed 2–3 hrs for chemiluminescence exposure. SDS-PAGE blots were exposed for 2–5 min. (**A**) The protein lysates from AD brains (cases no. 5–10) in BN-PAGE showed a high-molecular weight anti-$A\beta_{42}$-positive smear >1000 kD. Such smears were not observed in controls (cases no. 1–4). Synthetic $A\beta_{42}$ and $A\beta_{40}$ were loaded as positive and negative controls, respectively. In $A\beta_{42}$ preparations, long chemiluminescence exposure led to the detection of additional dimer and ~50 kD bands that were not observed after 2–5 min. exposures, as shown in Figure 3C. (**B**) The $A\beta_{42}$-positive material seen in (**A**) was not detectable in AD (cases no. 5–10) or in the controls (cases no. 1–4) in the native gel blotted with anti-$A\beta_{40}$ antibodies. Synthetic $A\beta_{42}$ and $A\beta_{40}$ were loaded as positive and negative controls, respectively. After 3 hrs of chemiluminescence exposure, synthetic $A\beta_{40}$ blots display a dimer band at ~10 kD in addition to the monomer band and the hiMWAβ smear already detected with shorter exposure times as depicted in Figure 3C. (**C**) The anti-$A\beta_{1-17}$ antibody also detected the high-molecular weight protein aggregates >1000 kD in the area of stacking gel in the protein lysate from AD brains (cases no. 5–10), which was not detectable in control brains (cases no. 1–4). In addition, anti-$A\beta_{1-17}$ also showed APP bands in AD and control cases (140–240 kD). (**D**) The APP-positive bands were confirmed with an antibody directed against N-terminal epitope of APP (22C11) in control (cases no. 1–4) and AD cases (cases no. 5–10). (**E**)–(**G**) SDS-PAGE analysis of AD brain protein lysates from cases no. 5–10 exhibited Aβ monomer and dimer bands with MBC-42 (**E**), MBC-40 (**F**) and anti-$A\beta_{1-17}$ (**G**) that were not detected in control brains (cases no. 1–4). The MBC-42-dimer (**E**) and 6E10-dimer bands (**G**) were not seen in all AD cases, whereas anti-$A\beta_{40}$ consistently detected dimer bands (**F**). A high-molecular smear was found in most AD cases with all three antibodies directed against Aβ. Interestingly, cases 6 and 10 exhibited nearly no SDS-stable hiMWAβ_{42} aggregates (**E**), whereas both cases showed high-molecular anti-$A\beta_{42}$-positive material in the BN-PAGE (**A**). (**H**) With the help of anti-$A\beta_{1-17}$ (6E10)-immunoprecipitation, monomer and dimer bands as well as loMWAβ (4–20 kD) smears and hiMWAβ (>160 kD) smears were visible in SDS-PAGE of AD brain lysates (cases no. 5–10) but not in those of controls (cases no. 1–4). The detection of the loMWAβ oligomers required chemiluminescence exposure for 3 hrs (*i.e.* long exposure times).

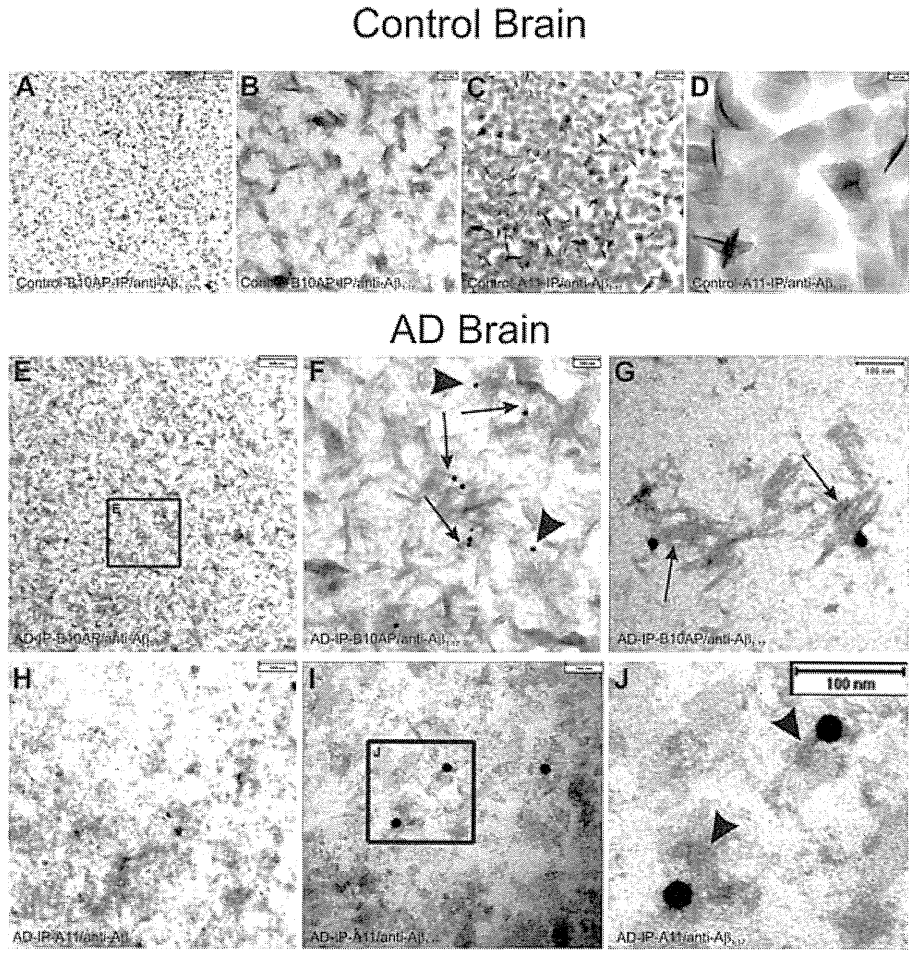

Fig. 2 Electron microscopic analysis of immunoprecipitated protein aggregates from AD and control brain as precipitated with B10AP-antibody fragments (B10AP-IP) and A11 antibodies (A11-IP). (**A**), (**B**) In the control case no. 3, protein aggregates were precipitated with B10AP, but anti-$A\beta_{1-17}$ did not show Aβ within these aggregates. There was also no non-specific labelling with anti-$A\beta_{1-17}$ because no gold particles were observed. The protein aggregates exhibited protofibril-aggregate-like architecture that is more evident at higher magnification (**B**). This indicates that B10AP does not specifically bind to Aβ protofibrils or fibrils but to proteins with a distinct protofibrillar/fibrillar conformation, as reported previously [2]. (**C**), (**D**) A11-IP from control cases resulted in detection of amorphous to spherical presumably oligomeric protein aggregates, as shown in control case no. 4, but did not exhibit Aβ as a component of these protein aggregates. There was also no non-specific labelling with anti-$A\beta_{1-17}$ because no gold particles were seen. The high magnification demonstrates the spherical shape of the precipitated proteins (**D**). Thus, A11 also binds spherical protein aggregates other than Aβ oligomers, as reported earlier by others [6]. (**E**), (**F**) B10AP-IP from AD brain lysate of case no. 7 showed protein aggregates of protofibril-like morphology. Immunogold labelling indicated $A\beta_{1-17}$-positive proteins. The frame in **E** indicates the areas enlarged in (**F**). At higher magnification, $A\beta_{1-17}$-positive material following B10AP-IP exhibited protofibril-like morphology (arrows in **F**) and less frequently amorphous structures (arrowheads in **F**). These types of Aβ aggregates prevailed in B10AP precipitates. (**G**) Only a few precipitated Aβ-positive protein aggregates exhibited fibrillar architecture (case no. 10) resembling synthetic Aβ fibrils (Fig. 3A, B). (**H**) A11-precipitated protein aggregates from AD case no. 7 exhibited spherical to amorphous morphology. Immunogold particles indicate the presence of $A\beta_{1-17}$-positive aggregates. (**I**)–(**J**) Similarly, A11-IP extracted mainly spherical and amorphous protein aggregates from AD case no. 10 shown here at higher magnification. Immunogold labelling indicated $A\beta_{1-17}$-positive proteins. The frame indicates the area enlarged in (**J**). The $A\beta_{1-17}$-positive aggregates observed after A11-IP showed a spherical shape (arrowheads in **J**).

that was not found in controls. Aβ monomers, dimers, or other loMWAβ species were not observed in AD cases or in controls (Fig. 1A). The high-molecular weight smear was also seen with anti-$A\beta_{1-17}$ at the level of stacking gel in AD cases (Fig. 1C) but not with anti-Aβ40 (Fig. 1B). However, the detection of synthetic $A\beta_{40}$ but not $A\beta_{42}$ indicated specific antibody function (Fig. 1B). Anti-$A\beta_{1-17}$ stained an additional 150–250 kD band (Fig. 1C) that was also observable with anti-APP antibodies, thereby indicating that this band represents APP-containing material (Fig. 1D). The APP-related band was also present in control cases, whereas the high-molecular weight anti-$A\beta_{1-17}$ smear was not seen (Fig. 1C). The BN-PAGE blots from brain samples were developed with a chemiluminescence exposure time of 2–3 hrs to detect even very minimal amounts of proteins.

SDS-PAGE with subsequent anti-$A\beta_{42}$, anti-$A\beta_{40}$ and anti-$A\beta_{1-17}$ Western blot analysis showed Aβ monomers and dimers in AD cases (Fig. 1E–G). Aβ aggregates with a molecular weight of >160 kD were observed in four of six cases with anti-$A\beta_{42}$ and a smear >260 kD was observed in all cases with anti-$A\beta_{1-17}$ (6E10) (Fig. 1E–G). After immunoprecipitation with anti-$A\beta_{1-17}$, a smear of hiMWAβ- (>160 kD) and loMWAβ aggregates (8–20 kD) as well as dimer bands at ~10 kD were consistently seen in AD

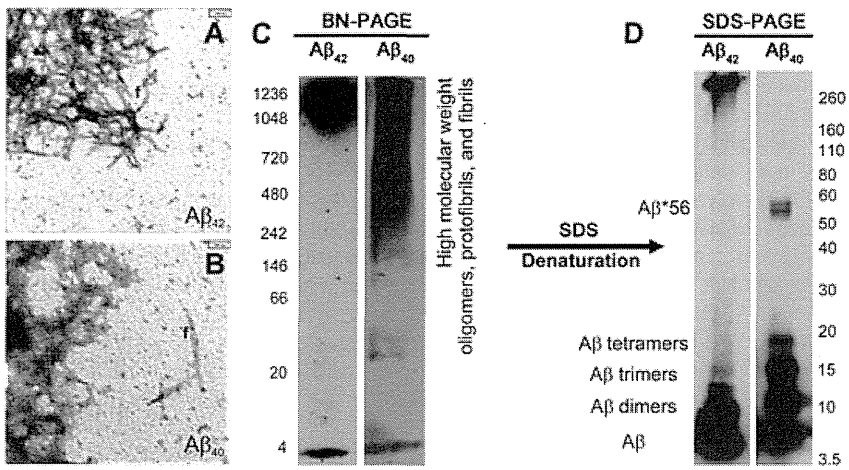

Fig. 3 Synthetic $A\beta_{42}$ (**A**) and synthetic $A\beta_{40}$ (**B**) dissolved in cell culture medium aggregated to amorphous oligomers, protofibrils and fibrils (f), as detectable by electron microscopy. (**C**) In BN-PAGE, a high-molecular weight smear occurred mainly above 700 kD in $A\beta_{42}$ preparations in addition to a distinct monomeric band at ~4 kD. $A\beta_{40}$ preparations produced a smear of Aβ aggregates with a molecular weight above 242 kD in addition to a clear monomeric band at ~4 kD. The BN-PAGE blots were developed with standard chemiluminescence exposure time of 2–5 min. Longer chemiluminescence exposure for 3 hrs resulted in additional loMWAβ bands depicted in Figure 1A and B, thereby indicating that these preparations contain low levels of these Aβ species as well. (**D**) In SDS-PAGE, hiMWAβ_{42} aggregates were strikingly reduced. Instead, the monomer, dimer and trimer bands displayed strong staining. Other loMWAβ_{42} oligomers were not evident. No hiMWAβ_{40} aggregates were seen after denaturing SDS-PAGE, but $A\beta_{40}$ monomer, dimer, trimer and tetramer bands as well as an Aβ*56 band were detectable at 56 kD.

cases (Fig. 1H). LoMWAβ and dimers were detected only after 3 hrs of chemiluminescence exposure but not in controls (Fig. 1H).

A11-antibody and B10AP-antibody fragments precipitate oligomeric and protofibrillar/fibrillar proteins including Aβ oligomers, Aβ protofibrils and Aβ fibrils in AD cases

In controls, immunoelectron microscopy of A11- and B10AP-precipitated proteins revealed a high number of precipitated and aggregated proteins that did not contain Aβ-positive material (Fig. 2A–D). There was no nonspecific labelling with anti-$A\beta_{1-17}$ in controls. B10AP-precipitated material exhibited a pattern that showed fibril-/ protofibril-like architectures (Fig. 2A, B) whereas the proteins precipitated by A11 displayed a spherical pattern (Fig. 2C, D).

In B10AP precipitates of the soluble fraction of AD brain homogenates, we observed protein aggregates with a fibril/protofibril-like pattern similar to that seen in controls. However, in AD brains a high number of Aβ-positive protein aggregates were detected with anti-$A\beta_{1-17}$ (Fig. 2E–G). High-magnification analysis of anti-$A\beta_{1-17}$-labeled protein aggregates revealed a protofibril-like pattern (Fig. 2F, arrows). However, a few amorphous protein aggregates (Fig. 2F, arrowheads) as well as fibrillar aggregates (Fig. 2G) were seen as well. Spherical Aβ oligomers were not observed following B10AP immunoprecipitation. Amorphous and spherical protein aggregates were observed after A11-immunoprecipitation from AD brain lysates. Anti-$A\beta_{1-17}$ antibodies detected protein aggregates of spherical and amorphous morphology (Fig. 2H–J). Protofibril-like structures as seen in B10AP precipitates were not observed in A11 precipitates.

SDS treatment destroys native high-molecular weight $A\beta_{42}$ and $A\beta_{40}$ aggregates

Synthetic $A\beta_{42}$ and $A\beta_{40}$ formed oligomeric and protofibrillar aggregates as detectable by electron microscopy (Fig. 3A, B). With 2–5 min. chemiluminescence exposure time, BN-PAGE blots revealed a monomer band and an additional prominent smear of $A\beta_{42}$- and $A\beta_{40}$ aggregates with a molecular weight >700 and 240 kD, respectively (Fig. 3C). However, after longer exposure time of 2–3 hrs, we observed smeary bands at ~10 and ~50 kD in $A\beta_{42}$ preparations, whereas $A\beta_{40}$ preparations exhibited an additional dimer band that was not detectable in short chemiluminescence exposure blots (Figs 1A, B, 3C). In SDS-PAGE, we observed few high-molecular weight aggregates above 240 kD in $A\beta_{42}$ preparations but not in $A\beta_{40}$ preparations, whereas very prominent Aβ monomer, dimer and trimer bands were observed for both synthetic $A\beta_{42}$- and $A\beta_{40}$ preparations. In SDS-treated $A\beta_{40}$ preparations, tetramer and Aβ*56 bands were present that were not seen in SDS-treated $A\beta_{42}$ preparations (Fig. 3D).

Discussion

Our results show that hiMWAβ_{42} oligomers and protofibrils with a molecular weight >1000 kD predominate in the soluble fraction of AD brain homogenates when these samples are analysed under native BN-PAGE conditions. $A\beta_{40}$ aggregates were not detected following BN-PAGE. Immunoelectron microscopy of immunoprecipitated oligomeric, fibrillar and protofibrillar proteins confirmed the presence of protofibrillar and spherical hiMWAβ aggregates in the soluble fraction of AD brain homogenates. These hiMWAβ

aggregates were not seen in controls, whereas analysis of control cases revealed that the A11 and B10AP antibodies/antibody fragments precipitate other proteins of similar morphology, and that only a portion of the precipitated proteins from AD cases were Aβ aggregates. Denaturation of the hiMWAβ aggregates by SDS resulted in the detection of Aβ monomers, dimers, and hiMWAβ with a molecular weight >160 kD in SDS-PAGE analysis of AD cases but not in controls. When using immunoprecipitation with anti-$Aβ_{1–17}$, a smear of loMWAβ and hiMWAβ was consistently seen following SDS-PAGE and subsequent Western blot analysis, thus indicating that dimers, trimers, tetramers and Aβ*56 are not the only Aβ oligomers that can be detected with SDS-PAGE as shown previously by other groups as well [4, 5]. These results lead us to conclude that, under native conditions, Aβ monomers and loMWAβ aggregates, such as dimers, trimers and Aβ*56, do not represent the major pool of Aβ aggregates in the human AD brain. More likely, loMWAβ aggregates may occur transiently during aggregation or after denaturation of hiMWAβ. The strongest argument in favour of this hypothesis is our finding that hiMWAβ oligomer preparations and Aβ protofibril preparations of synthetic $Aβ_{42}$- and $Aβ_{40}$ peptides did not exhibit high levels of loMWAβ oligomers in BN-PAGE but did so in SDS-PAGE. Moreover, subsequent to SDS-induced protein denaturation, hiMWA$β_{40}$ aggregates were no longer seen and synthetic hiMWA$β_{42}$ aggregates were remarkably reduced. A possible argument against the predominance of hiMWAβ in the soluble fraction is that Aβ monomers tend to aggregate in the presence of oligomers [24] and that this occurs during protein preparation. Nevertheless, in synthetic Aβ preparations with high amounts of aggregated Aβ, we detected a significant monomer band after BN-PAGE. This may indicate that Aβ monomers in the soluble brain lysates remained stable during the process of native protein preparation. As such, it is likely that the hiMWA$β_{42}$ aggregates observed in the native soluble fraction indeed represent the major form of soluble Aβ in the human AD brain.

Our finding that $Aβ_{40}$ was detected in AD cases in SDS-PAGE but not in BN-PAGE could be attributable either to a lower resolution of native gels in comparison to that of denaturing gels or to the fact that a potential smear of $Aβ_{40}$ aggregates falls far below detectable levels. Presumably, SDS treatment denatures all kinds of $Aβ_{40}$ oligomers and, in so doing, leads to the accumulation of $Aβ_{40}$ monomers in a single band. Thus, a non-detectable $Aβ_{40}$ smear in BN-PAGE might be converted into a detectable well-defined band in the SDS-PAGE. This hypothesis is supported by our finding of a detectable hiMWA$β_{40}$ smear in synthetic $Aβ_{40}$ preparation that disappeared after SDS treatment and converted into strongly stained monomer and loMWAβ oligomer bands. In BN-PAGE, the spectrum of synthetic hiMWA$β_{40}$ oligomers was greater (>240 kD) than that of synthetic hiMWA$β_{42}$ oligomers (>700 kD). This suggests that the concentrations of distinct hiMWA$β_{40}$ oligomers are lower than those of distinct hiMWA$β_{42}$ oligomers because of the more widespread distribution of hiMWA$β_{40}$ aggregates in the gel. As a result, hiMWA$β_{40}$ oligomers and may be less easily detected in native brain lysates. An alternative explanation, on the other hand, could be that $Aβ_{40}$ interacts with other proteins that hide its C-terminus. In addition, the predominance of hiMWA$β_{42}$ in the native soluble fraction of the AD brains investigated here confirms previous reports of a predominant occurrence of $Aβ_{42}$ in parenchymal soluble and insoluble Aβ aggregates in AD [25, 26].

At first, the results reported here appear to contradict the findings of other authors, who argue that distinct loMWAβ oligomers, such as dimers and Aβ*56, are critical for the development of AD [3, 9, 27]. These authors provide evidence that loMWAβ oligomer preparations received by size-exclusion chromatography are detectable in human as well as transgenic mouse brains, and are capable of inducing cognitive deficits in the rat [9] or altering long-term potentiation [3]. Given our *in vitro* and *in vivo* findings, however, one could also speculate that small amounts of loMWAβ oligomers (possibly resulting from the denaturation of hiMWAβ oligomers, protofibrils and fibrils) either are critical for the development of AD or that, upon their administration, loMWAβ oligomers may spontaneously aggregate and form hiMWAβ oligomers, as appears to be the case based upon our native gel analysis of $Aβ_{40}$- and $Aβ_{42}$ preparations and the results of Nguyen *et al.* [24], who showed that Aβ oligomers accommodate added Aβ monomers. Thus, hiMWAβ aggregates contribute to the pathogenesis of AD either on its own or do so indirectly by providing the reservoir of hiMWAβ aggregates that denature and, in so doing, release loMWAβ oligomers.

That Aβ aggregates, including Aβ plaques, dissociate during the pathogenesis of AD is corroborated by the finding that in late-stage AD cases plaque frequency is lower than in earlier stages [28]. The relevance of soluble hiMWAβ for the pathogenesis of AD may be further supported by the finding of neuritic degeneration near Aβ plaques, *i.e.* in areas with high levels of hiMWAβ presumably dissolved from Aβ plaques, in the APP transgenic mouse brain [7, 8, 29], in aged rhesus monkeys [30] and in the AD brain [31], and also by the finding that dendritic degeneration in another APP-transgenic mouse model begins at the same time as the deposition of initial diffuse Aβ-plaques, *i.e.* when hiMWAβ aggregates begin to predominate in the cortex [32].

Here, the stability of hiMWA$β_{42}$ aggregates was greater than that of $Aβ_{40}$ aggregates in *in vitro* experiments, thus confirming previous reports that soluble $Aβ_{42}$ aggregates are more stable than $Aβ_{40}$ aggregates [33, 34]. Taken together with our finding that hiMWA$β_{42}$ aggregates predominate in the native soluble fraction of the brain, it may be speculated that it is the stability of soluble $Aβ_{42}$ aggregates in the soluble compartment of the brain that accounts for its predominance in parenchymal Aβ plaque deposition [26].

In conclusion, the results of the present study strongly suggest that hiMWAβ oligomers, protofibrils and fibrils are the predominant soluble Aβ aggregates in the AD brain. loMWAβ oligomers in high concentrations are detectable only after denaturation of hiMWAβ aggregates. In view of the denaturation of hiMWAβ aggregates and fibrils into loMWAβ oligomers, we propose that Aβ plaques consisting of both fibrillar Aβ as well as soluble

hiMWAβ aggregates may serve as reservoirs for the release of loMWAβ oligomers.

Acknowledgement

We thank Kelly Del Tredici, M.D., Ph.D. (University of Ulm, Department of Neurology, Center for Clinical Research) for reading the final version of the revised manuscript.

Conflict of interest

D.R.T. received research grants from the Deutsche Forschungsgemeinschaft (DFG-grant TH624/6–1) and from the Alzheimer Forschung Initiative (AFI Grant #10810). M.F. was supported by the Deutsche Forschungsgemeinschaft (SFB 610) and the Landesexzellenz-Netzwerk Biowissenschaften. There are no other conflicts of interest.

References

1. **Masters CL, Simms G, Weinman NA, *et al.*** Amyloid plaque core protein in Alzheimer disease and Down syndrome. *Proc Natl Acad Sci USA.* 1985; 82: 4245–9.
2. **Habicht G, Haupt C, Friedrich RP, *et al.*** Directed selection of a conformational antibody domain that prevents mature amyloid fibril formation by stabilizing Abeta protofibrils. *Proc Natl Acad Sci USA.* 2007; 104: 19232–7.
3. **Shankar GM, Li S, Mehta TH, *et al.*** Amyloid-beta protein dimers isolated directly from Alzheimer's brains impair synaptic plasticity and memory. *Nat Med.* 2008; 14: 837–42.
4. **Rosen RF, Ciliax BJ, Wingo TS, *et al.*** Deficient high-affinity binding of Pittsburgh compound B in a case of Alzheimer's disease. *Acta Neuropathol.* 2010; 119: 221–33.
5. **Rosen RF, Tomidokoro Y, Ghiso JA, *et al.*** SDS-PAGE/immunoblot detection of Abeta multimers in human cortical tissue homogenates using antigen-epitope retrieval. *J Vis Exp.* 2010; 38: doi: 10.3791/1916.
6. **Kayed R, Head E, Thompson JL, *et al.*** Common structure of soluble amyloid oligomers implies common mechanism of pathogenesis. *Science.* 2003; 300: 486–9.
7. **Spires TL, Meyer-Luehmann M, Stern EA, *et al.*** Dendritic spine abnormalities in amyloid precursor protein transgenic mice demonstrated by gene transfer and intravital multiphoton microscopy. *J Neurosci.* 2005; 25: 7278–87.
8. **Tsai J, Grutzendler J, Duff K, *et al.*** Fibrillar amyloid deposition leads to local synaptic abnormalities and breakage of neuronal branches. *Nat Neurosci.* 2004; 7: 1181–3.
9. **Lesne S, Koh MT, Kotilinek L, *et al.*** A specific amyloid-beta protein assembly in the brain impairs memory. *Nature.* 2006; 440: 352–7.
10. **Thal DR, Papassotiropoulos A, Saido TC, *et al.*** Capillary cerebral amyloid angiopathy identifies a distinct APOE epsilon4-associated subtype of sporadic Alzheimer's disease. *Acta Neuropathol.* 2010; 120: 169–83.
11. **American Psychiatric Association.** Diagnostic and statistical manual of mental disorders. 4th ed. Washington DC: American Psychiatric Association; 1994.
12. **The National Institute on Aging.** Consensus recommendations for the postmortem diagnosis of Alzheimer's disease. The National Institute on Aging, and Reagan Institute Working Group on Diagnostic Criteria for the Neuropathological Assessment of Alzheimer's Disease. *Neurobiol Aging.* 1997; 18: S1–2.
13. **Insausti R, Amaral DG.** Hippocampal Formation. In: Paxinos G, Mai JK, editors. The human nervous system. 2nd ed. London: Elsevier; 2004. pp. 872–914.
14. **Braak H, Alafuzoff I, Arzberger T, *et al.*** Staging of Alzheimer disease-associated neurofibrillary pathology using paraffin sections and immunocytochemistry. *Acta Neuropathol.* 2006; 112: 389–404.
15. **Kim KS, Miller DL, Sapienza VJ, *et al.*** Production and characterization of monoclonal antibodies reactive to synthetic cerebrovascular amyloid peptide. *Neurosci Res Commun.* 1988; 2: 121–30.
16. **Braak H, Braak E.** Neuropathological stageing of Alzheimer-related changes. *Acta Neuropathol.* 1991; 82: 239–59.
17. **Mirra SS, Heyman A, McKeel D, *et al.*** The Consortium to Establish a Registry for Alzheimer's Disease (CERAD). Part II. Standardization of the neuropathologic assessment of Alzheimer's disease. *Neurology.* 1991; 41: 479–86.
18. **Thal DR, Rüb U, Schultz C, *et al.*** Sequence of Abeta-protein deposition in the human medial temporal lobe. *J Neuropathol Exp Neurol.* 2000; 59: 733–48.
19. **Thal DR, Rüb U, Orantes M, *et al.*** Phases of Abeta-deposition in the human brain and its relevance for the development of AD. *Neurology.* 2002; 58: 1791–800.
20. **Utter S, Tamboli IY, Walter J, *et al.*** Cerebral small vessel disease-induced apolipoprotein E leakage is associated with Alzheimer disease and the accumulation of amyloid beta-protein in perivascular astrocytes. *J Neuropathol Exp Neurol.* 2008; 67: 842–56.
21. **Yamaguchi H, Sugihara S, Ogawa A, *et al.*** Diffuse plaques associated with astroglial amyloid beta protein, possibly showing a disappearing stage of senile plaques. *Acta Neuropathol.* 1998; 95: 217–22.
22. **Weidemann A, Konig G, Bunke D, *et al.*** Identification, biogenesis, and localization of precursors of Alzheimer's disease A4 amyloid protein. *Cell.* 1989; 57: 115–26.
23. **Huang X, Atwood CS, Moir RD, *et al.*** Trace metal contamination initiates the apparent auto-aggregation, amyloidosis, and oligomerization of Alzheimer's Abeta peptides. *J Biol Inorg Chem.* 2004; 9: 954–60.
24. **Nguyen PH, Li MS, Stock G, *et al.*** Monomer adds to preformed structured oligomers of Abeta-peptides by a two-stage dock-lock mechanism. *Proc Natl Acad Sci USA.* 2007; 104: 111–6.
25. **Murphy MP, Beckett TL, Ding Q, *et al.*** Abeta solubility and deposition during AD progression and in APPxPS-1 knock-in mice. *Neurobiol Dis.* 2007; 27: 301–11.
26. **Roher AE, Lowenson JD, Clarke S, *et al.*** beta-Amyloid-(1–42) is a major component of cerebrovascular amyloid deposits: implications for the pathology of Alzheimer disease. *Proc Natl Acad Sci USA.* 1993; 90: 10836–40.
27. **Reed MN, Hofmeister JJ, Jungbauer L, *et al.*** Cognitive effects of cell-derived and synthetically derived Abeta oligomers.

Neurobiol Aging. 2009: doi:10.1016/j.neurobiolaging.2009.11.007.

28. **Thal DR, Arendt T, Waldmann G, *et al.*** Progression of neurofibrillary changes and PHF-tau in end-stage Alzheimer's disease is different from plaque and cortical microglial pathology. *Neurobiol Aging.* 1998; 19: 517–25.
29. **Meyer-Luehmann M, Spires-Jones TL, Prada C, *et al.*** Rapid appearance and local toxicity of amyloid-beta plaques in a mouse model of Alzheimer's disease. *Nature.* 2008; 451: 720–4.
30. **Shah P, Lal N, Leung E, *et al.*** Neuronal and Axonal Loss Are Selectively Linked to Fibrillar Amyloid-{beta} within Plaques of the Aged Primate Cerebral Cortex. *Am J Pathol.* 2010; 177: 325–33.
31. **Serrano-Pozo A, William CM, Ferrer I, *et al.*** Beneficial effect of human anti-amyloid-beta active immunization on neurite morphology and tau pathology. *Brain.* 2010; 133: 1312–27.
32. **Capetillo-Zarate E, Staufenbiel M, Abramowski D, *et al.*** Selective vulnerability of different types of commissural neurons for amyloid beta-protein induced neurodegeneration in APP23 mice correlates with dendritic tree morphology. *Brain.* 2006; 129: 2992–3005.
33. **Lambert MP, Barlow AK, Chromy BA, *et al.*** Diffusible, nonfibrillar ligands derived from Abeta1–42 are potent central nervous system neurotoxins. *Proc Natl Acad Sci USA.* 1998; 95: 6448–53.
34. **Levine H 3rd.** Soluble multimeric Alzheimer beta(1–40) pre-amyloid complexes in dilute solution. *Neurobiol Aging.* 1995; 16: 755–64.